Comparison of different models for high damping rubber bearings in seismically isolated bridges

E. Tubaldi[1], S. A. Mitoulis[2], H. Ahmadi[3]

[1] Department of Civil and Environmental Engineering, Imperial College London, London, UK; email: etubaldi@gmail.com;
[2] Department of Civil and Environmental Engineering, Faculty of Engineering and Physical Sciences, University of Surrey, Guildford, Surrey GU2 7XH, United Kingdom, email: s.mitoulis@surrey.ac.uk
[3] Tun Abdul Razak Research Centre (TARRC), Brickendonbury, Brickendon Lane, Hertford, UK, email: hahmadi@tarrc.co.uk

SUMMARY

Steel-reinforced high damping natural rubber (HDNR) bearings are widely employed in seismic isolation applications to protect structures from earthquake excitations. In multi-span simply supported bridges, the HDNR bearings are typically placed in two lines of support, eccentric with respect to the pier axis. This configuration induces a coupled horizontal-vertical response of the bearings, mainly due to the rotation of the pier caps. Although simplified and computationally efficient models are available, which neglect the coupling between the horizontal and vertical response, their accuracy has not been investigated to date.

In this paper, the dynamic behaviour and seismic response of a benchmark three-span bridge are analysed by using an advanced HDNR bearing model recently developed and capable of accounting for the coupled horizontal and vertical responses, as well as for significant features of the hysteretic shear response of these isolation devices. The results of the analyses shed light on the importance of the bearing vertical stiffness and how it modifies the seismic performance of isolated bridges. Successively, the seismic response estimates obtained by using simplified bearing models, whose use is well established and also suggested by design codes, are compared against the corresponding estimates obtained by using the advanced bearing model, to evaluate their accuracy for the current design practice.

Keywords: Seismic isolation; Bridges; Multi-span simply-supported (MSSS) deck; High damping natural rubber (HDNR) bearings; Vertical behaviour; Simplified models.

INTRODUCTION

Steel-reinforced high damping natural rubber (HDNR) bearings are widely used in bridges to protect them against earthquakes. These bearings consist of alternating layers of filled natural rubber that provide period elongation and energy dissipation and reinforcing steel shims, which enhance the vertical bearing capacity. HDNR bearings have been proven to be efficient isolation devices based on their satisfactory performance during major earthquakes [1]-[5] and by the numerous experiments carried out on the rubber material [6]-[8] and the bearings (see e.g. [9]-[11]). In isolated bridges and buildings, HDNR bearings are designed to sustain compressive loads due to the self-weight and the live loads acting on the superstructure, and also horizontal loads imposed by earthquakes and/or wind. In the recent years analytical models have been developed to accurately describe the behaviour under shear for constant vertical loads [8]-[11]. However, under certain design situations, the bearings may be subjected to uplift, i.e. tensile forces. This condition has been documented and investigated by Ryan and Chopra [12] for isolated buildings. Bearing may also experience uplift in bridges (e.g., in [13]), and particularly in those with simply supported deck spans [14]-[15]. In the latter case, the bearings are typically placed eccentrically with respect to the vertical axis of the piers and the longitudinal seismic motion of the deck induces rotation of the pier cap about the transverse axis, which in turn causes either tensile (uplift) or compressive deformations to the bearings. Vertical axial forces may also be increased by the motion of the deck, which can be excited in the vertical direction, even if the vertical seismic component is neglected. The vertical forces on the bearings could reach a critical level, as HNDR bearings may undergo cavitation for relatively low values of the tensile stresses [16]. The post-cavitation behaviour of the bearings is characterised by very low stiffness and by potential local damage of the isolator [17]-[18]. Also, compressive forces imposed on the isolators by the pier rotations, may cause buckling, especially when they are coupled with large shear deformations [19].

Despite the importance of the aforementioned axial loading of the isolators, the vertical behaviour of the bearings is usually ignored. For example, in Siqueira et al. [20] the isolators were assumed to

be rigid in the vertical direction. Cardone et al. [21] and Jara et al. [22] did not describe the modelling of the vertical behaviour of the bearings, whereas in Zanardo et al. [23] and in Matsagar and Jangid [24] a linear elastic spring was used for the vertical direction of the isolator, which is uncoupled from the other springs describing the response in shear. Furthermore, although current design guidelines require the bearings to be checked against uplift and buckling [25]-[29], no guidance is provided for modelling the vertical behaviour of isolators, whereas the use of the equivalent visco-elastic or bilinear hysteretic models is prescribed for simulating the shear response of bearings only.

The uplift effect of the HDNR bearings of a benchmark isolated bridge with prestressed I-beam girders, typical of bridge types met in Southern Europe, was recently studied by Mitoulis [14], yet the bearings were described with linear elastic models, which did not consider the coupling of the vertical and horizontal response. In Tubaldi et al. [15], a parametric study was carried out to identify under which design situations unfavourable limit states related to the bearing performance may occur in multi-span simply-supported isolated (MSSS) bridges with HDNR bearings placed eccentrically with respect to the pier axis. Based on the use of advanced bearing models, the study showed that excessive tensile stresses or buckling of the isolators are strongly dependent on the bearing design and in particular on the bearing shape factor. However, the latter paper considered only the horizontal component of the earthquake input, and did not investigate the importance of employing simplified modelling approaches, recurrent in design practice [30], on the estimate of the bridge performance.

In this study, the modelling of HDNR isolation bearings is studied by evaluating the dynamic behaviour and seismic response of a benchmark MSSS bridge, with the bearing modelled by means of both advanced and simplified models. The advanced bearing model, recently developed by Kumar et al. [18], has appropriate features, required for this investigation, such as the nonlinear amplitude-dependent behaviour in shear that fits accurately with characterisation test results, the coupling of vertical and horizontal motion and the variation of the critical buckling load capacity,

82 due to the lateral displacement and the cavitation and global post-cavitation behaviour in tension
83 with stiffness degradation in cyclic tensile loading due to cavitation. The simplified bearing models
84 on the other hand use elasto-plastic or visco-elastic springs to describe the shear response, and
85 linear elastic springs whose response is uncoupled from the shear response to describe the axial
86 behaviour. It is noteworthy that the accuracy of these simplified models for describing the response
87 of isolation bearing in shear has been investigated in the literature [31]-[33], but by considering
88 single bearings subjected to displacement-controlled tests [32], or simplified single degree of
89 freedom (SDOF) systems [31], or bridge typologies other than that considered in this study [33].
90 Moreover, in studies considering MSSS isolated bridges (e.g., [34]), the accuracy of linearization
91 procedures is evaluated by looking only at the estimate of the displacement response of the pier and
92 the deck. Thus, to the authors' best knowledge, the vertical bearing response in isolated bridges, the
93 coupling with the horizontal response, and its modelling, have not received sufficient attention to
94 date. Hence, one of the aim of this study is to assess whether simplified approaches for modelling
95 the behaviour of rubber bearings under combined shear and vertical actions are accurate or not for
96 evaluating the performance of the bridge components and not only the displacement demand of the
97 deck. The bridge typology considered herein is appropriate for this purpose because it is
98 characterized by a significant coupling between horizontal and vertical response.
99 In order to provide insight into the relevance of the problem, in the first part of the paper the
100 dynamic and seismic behaviour of the case study is analyzed in depth by employing the advanced
101 bearing model. The bearing model parameters are calibrated to fit the data of an experimental
102 campaign carried out at the laboratories of Tun Abdul Razak Research Centre in the UK (TARRC)
103 on double shear test pieces with the aim of characterising the HDNR response in shear. Soil
104 structure interaction (SSI) effects are also taken into account, since they have proven to have an
105 important effect on the structural response of isolated bridges in general as well as MSSS bridges
106 [35]- [37]. A wide set of response parameters of importance for the performance assessment of the
107 bridge components are monitored, for different values of the shape factor S_r, controlling the vertical

bearing stiffness. Subsequently, the bridge seismic response estimates obtained by using the advanced and the simplified HDNR bearing models are compared against each other and the significance of detailed modelling of the bearings to evaluate the performance of the bridge critical components, i.e. the piers, the foundations, the bearings and the deck, is highlighted.

A set of 7 spectrum-compatible ground motion records is considered for the seismic analyses. While the assessment of the relative accuracy of the bearing models is carried out by considering both the horizontal and the vertical component of the seismic input, some results obtained by considering only the longitudinal component are also presented to highlight the fact that a significant vertical response may arise even if the vertical ground acceleration is disregarded.

DESCRIPTION OF THE BENCHMARK BRIDGE

The benchmark bridge is a reinforced concrete regular bridge with three spans of equal lengths and solid circular homogeneous bridge piers. This bridge, whose geometrical and mechanical properties are representative of many bridges in Europe with simply-supported pre-cast and pre-stressed concrete I-beams supported on steel-laminated HDNR bearings. Fig. 1 illustrates the bridge elevation and the deck section at the midspan. Each precast beam is seated on the intermediate reinforced concrete piers and on the seat-type abutments through HDNR bearings. A total of five bearings per line of support are considered, hence five bearings are placed on the abutments and 10 bearings on the piers. The two lines of isolators at mid-supports are placed eccentrically with respect to the pier axis. The simply-supported deck spans are connected by a cast-in-situ continuity slab, which is reinforced with ordinary reinforcement. This connection enables a continuous deck surface to be achieved, thus avoiding the use of expansion joints over the piers. However, despite this connection, the bridge still behaves as if it is consisted of a series of simply-supported beams under the vertical loads, provided that the slab is sufficiently flexible to accommodate the rotations of the adjacent deck segments. Expansion joints allow for thermal contraction and expansion of the deck at the abutments.

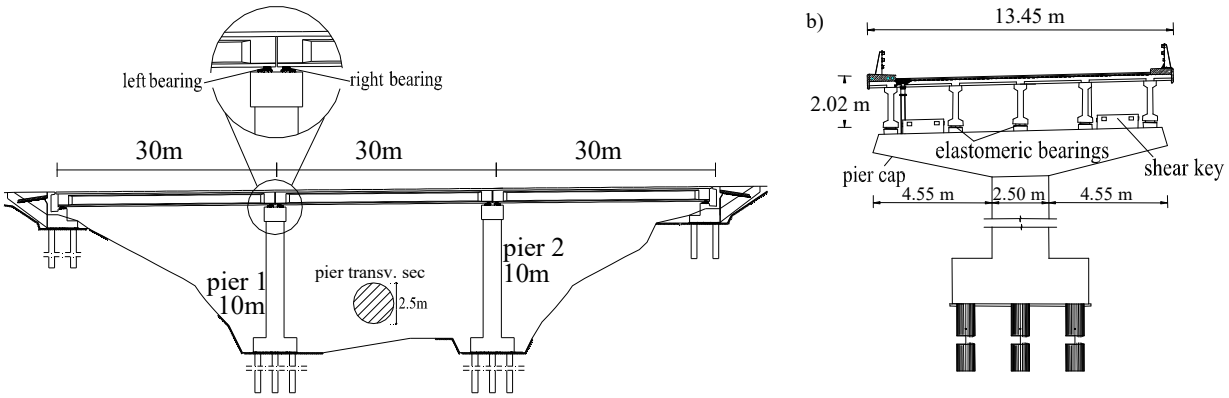

Fig. 1. a) Bridge elevation and b) deck section at midspan.

The deck span length is L_{sp}=30 m, the transverse section width is 13.5m, whereas the carriageway width is assumed 11.5 m, corresponding to three nominal lanes according to Eurocode 1 [38]. The length of the continuity slab is L_{cs} = 0.5 m. The mass per unit length, accounting for 20% of the traffic loads, is equal to 25.35 t/m. The piers have a circular cross section with diameter of 2.5 m and height of 10 m. The longitudinal reinforcement consists of 93 bars of 26 mm, whereas the transverse reinforcement of ∅ 14 mm and spacing of 100 mm. The class of concrete is C30/40, whereas the class of steel is S355. The cap beam has height of 1.35 m, the transverse section has width along the longitudinal and transverse direction equal respectively to 3.0 m and 12.5 m.

The foundations of the bridge piers consist of a 3×3 group of piles, whereas the soil profile consists of a deformable soil layer overlying a very dense sand deposit. The deformable deposit has a depth of 15 m, shear wave velocity V_{s1} = 200m/s and density ρ_{s1} = 1.7t/m^3. The dense sand deposit is characterised by shear wave velocity V_{s2}=800m/s and density ρ_{s2}=2.5t/m^3. Poisson's ratio is considered to be ν_s = 0.4 and material hysteretic damping ξ_s = 10%, which is compatible with the design level of strain in the soil. The concrete piles have a Young's modulus of $3 \cdot 10^7$ kN/m^2 and density of 2.5t/m^3. The piles are 18.0 m long, have a circular cross sections of 0.8 m diameter and a spacing of three diameters, i.e. 2.4 m centre to centre distance. The average shear wave velocity of the most superficial 30 m layers of soil equal to 320 m/s. Thus, the soil type is classified as C according to EC8-Part 1 [25], corresponding to a soil factor S = 1.15. The peak ground acceleration expected at the site is assumed equal to PGA = 0.4Sg.

153 The isolation system consists of a total of 30 identical HDNR bearings supporting a total of 15
154 prefabricated beams of the deck. The bearing eccentricity, measured from centre of the bearings to
155 pier axis, is e_b=0.8 m in the longitudinal direction of the bridge. The HDNR compound is a medium
156 compound developed at TARRC, which passes all the characterisation tests of EN15129 [27]. The
157 bearing properties have been chosen by employing a displacement-based design approach, similar
158 to that proposed in [21]. The flexibility and mass of the piers have been neglected, given their
159 limited contribution to the isolated system response, and the target values of the displacement
160 demand for the bearings and relevant shear deformation of the rubber have been assumed equal
161 respectively to 0.264 m and γ_{Ed} =1.5. At this deformation level, the equivalent properties of the
162 rubber are: ξ_{is} = 10.8% the damping ratio, and G_{eff} = 700 kPa the effective shear modulus. Using the
163 EC8-2 Type 1 response spectrum [25], reduced to account for the added isolators damping ratio, a
164 value of the target vibration period of T_{is} = 2.0 s is obtained. Given the total mass of the
165 superstructure of M_{tot} = 2281.6 t, the horizontal stiffness to be provided by each of the 30 isolators
166 is $k_h = \frac{4\pi^2 M_{tot}}{30T^2}$ = 750.6 kN/m. Having assumed γ_{Ed} =1.5, the total rubber height must be T_r =
167 0.27/1.5 = 0.18 m, and the rubber area required to achieve the target stiffness is $A_r = k_h T_r / G_{eff}$ =
168 0.193 m, corresponding to a diameter D_r = 0.50 m. The assumed value of the bearing shape factor is
169 $S_r = D_r / 4t_r$ =15, leading to a thickness of the single rubber layer of t_r = 8 mm, and a total number of
170 rubber layers n_r = 22. The assumed value of the shim plate thickness is t_s = 5 mm.
171 The bearing design ensures that all the safety verifications required by EC8-2 [26] as well as
172 EN15129 [27] and EN1337-3 [28] are satisfied. These checks concern the performance of the
173 bearings under both the seismic and the non-seismic loading conditions. Further information about
174 the limit states considered for the design can be found in [15].

175 # MODELLING OF THE ISOLATED BRIDGE

176 The dynamic behaviour and seismic response of the bridge in the longitudinal direction are

analyzed with a finite element model (Fig. 2) built in OpenSees [39] by following the guidelines of Kappos et al. [40]. Both the superstructure and the substructures are modelled by a spine of linear beam-column elements with lumped nodal masses, spanning between successive nodes along the elements length. The spine follows the centre of gravity of the cross section along the length of the element it represents. All the components of the bridge are discretised into a sufficient number of elements in order to accurately describe the actual mass distribution and the influence of higher vibration modes.

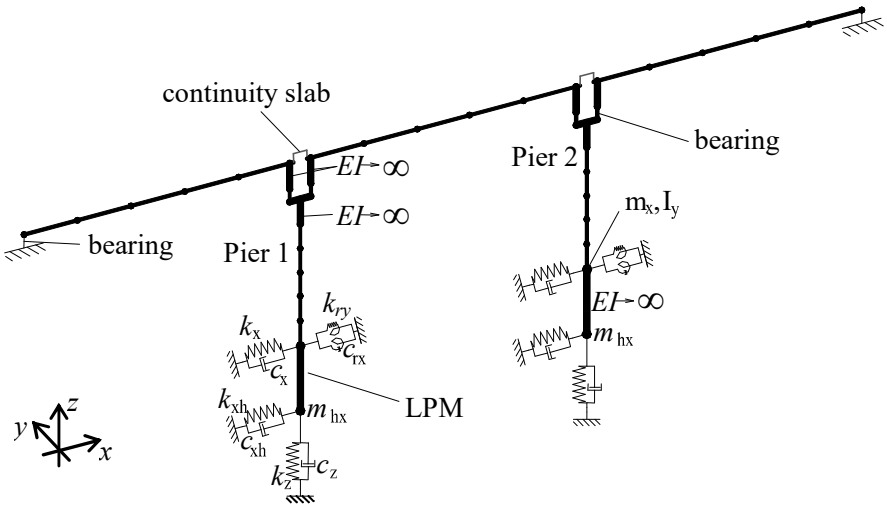

Fig. 2. FE model of the isolated bridge.

The deck is modelled by linear elastic frame elements considering uncracked stiffness, as it is prestressed and, thus, it is not expected to undergo flexural cracking. However, for the continuity slab an effective stiffness, equal to 40% of the gross stiffness, is used to simulate the expected cracking. The piers are modelled by linear elastic frame elements. The assumption of linear elastic behaviour is based on the fact that the bridge is isolated and, thus, the piers are designed to respond in an elastic or essentially-elastic manner. Furthermore, although the piers are subjected to compressive actions due to the vertical loads, they are expected to undergo some level of cracking. Thus, a cracked effective stiffness is employed to describe their flexural behaviour. During the analysis, a check is performed to make sure that the yield strength of the piers is not exceeded. Based on moment-curvature analysis of the pier base section, the effective cracked stiffness, secant to the yield point, is assumed equal to approximately $0.5EI_g$, where EI_g is the gross stiffness.

197 The inelastic deformations and the relevant hysteretic dissipation of energy is concentrated within
198 the isolators. The viscous damping of the system, representing energy dissipation sources other than
199 that of the isolators, is taken into account by assigning a Rayleigh damping to the piers nodes only,
200 i.e., the viscous damping matrix has non-null terms only in correspondence of these nodes. Hence, a
201 damping ratio of approximately 5% is provided to the higher modes related to the vibration of the
202 pier only.
203 The effects of soil-structure interaction on the structural response are usually divided into two
204 phenomena: a) kinematic interaction and b) inertial interaction [41]-[43]. This study does not
205 account for the kinematic effects on the foundation input motion and thus the free-field motion, as
206 described by a set of natural ground motion, is directly used as input motion. This choice is based
207 on the fact that isolated bridges are excited by relatively low frequencies, and thus the error
208 resulting from neglecting the kinematic SSI effects is expected to be negligible [35]-[37]. However,
209 it should be noted that the neglected rocking motion generated by kinematic interaction may
210 contribute to the coupled horizontal-vertical response of the bearings, and this is something that is
211 not analysed herein because it would require also a more complicated model of the soil-foundation
212 system, which is considered to be out of the scope of the paper.
213 The inertial effects of SSI are accounted for by employing Lumped Parameter Models (LPMs)
214 approach. These LPMs are a set of translational and rotational springs, dampers and masses that
215 permit to reproduce, in the time domain, the frequency-dependent compliance of the soil-foundation
216 system (Fig. 2). The properties of the LPMs are derived by employing the approach outlined in Dezi
217 et al. [44], based on simplified formulas calibrated from results of an extensive non-dimensional
218 parametric analysis considering head-bearing pile groups. The proposed approach allows to
219 accurately simulate the compliance of pile foundations and important features of the soil-foundation
220 system behaviour such as the coupled rotational-translational response. The piles are fully
221 embedded in the soil, socketed into the sand deposit and connected at the heads by a cap.
222 Having considered a seismic input along the longitudinal direction, the bridge exhibits a non-null

response only in the longitudinal plane (i.e., plane xz of Fig. 2) and thus few components of the impedance matrix $\tilde{\mathfrak{I}}(\omega)$ of the LPM are significant for the problem studied. Table 1 reports the values of the properties of the LPM illustrated in Fig. 2b and Fig. 3 illustrates the variation with the frequency of the real and imaginary part of the significant components of $\tilde{\mathfrak{I}}(\omega)$.

Table 1. Values of the LPM.

k_x	c_x	m_x	k_{ry}	c_{ry}	I_y	k_z	c_z	m_z	k_{xh}	c_{xh}	m_{xh}
kN/m	kNs/m	kNs^2/m	kNm/rad	kNms/rad	kNms^2/rad	kN/m	kNs/m	kNs^2/m	kN/m	kNs/m	kNs^2/m
1.32E+05	8.95E+03	58.16	4.62E+07	9.97E+04	649.71	7.48E+06	6.91E+04	102.69	7.48E+06	6.91E+04	102.69

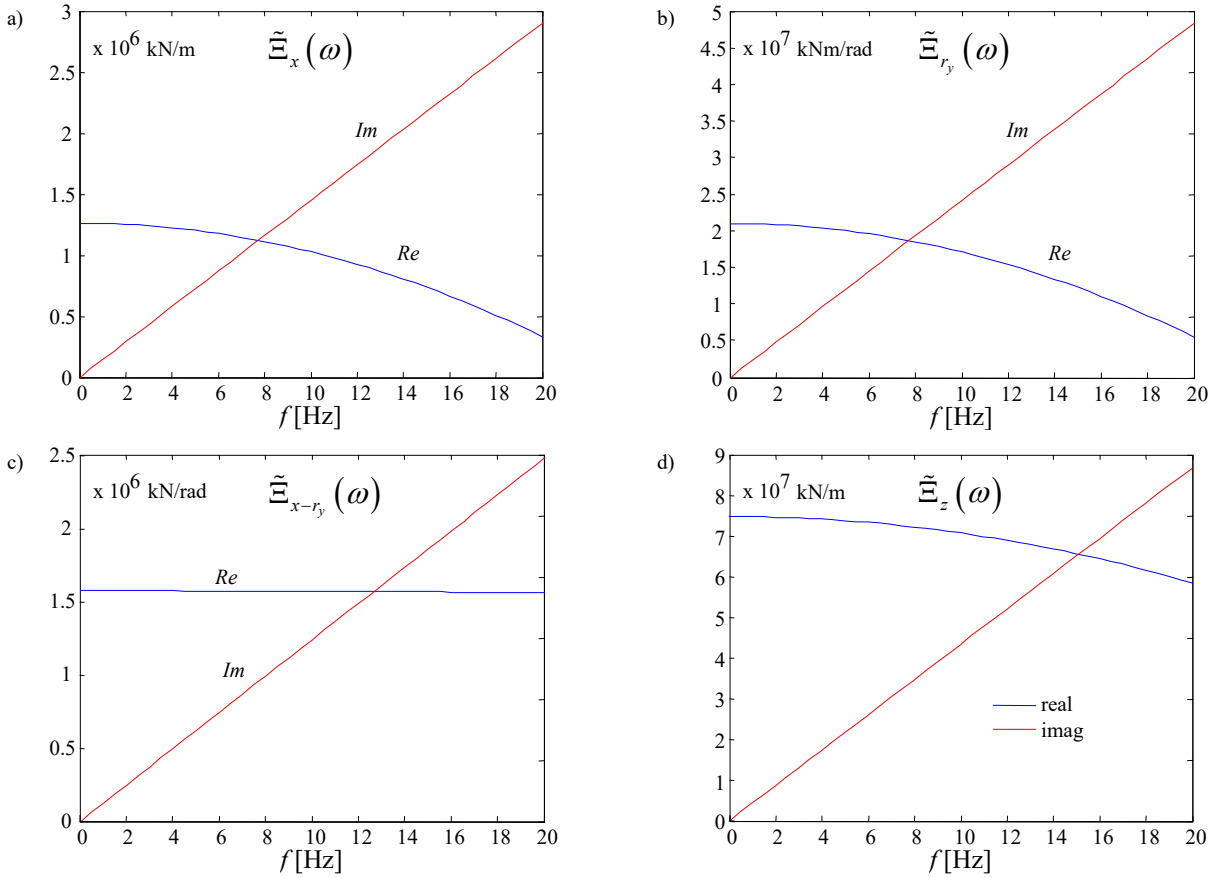

Fig. 3. Variation with frequency f of most relevant components of the impedance matrix: a) translation along x, b) rotation with respect to y , c) interaction between translation along x and rotation with respect to y, d) translation along z.

It is noteworthy that the LPMs comprise masses which are directly excited by the earthquake acceleration. These masses alter the dynamic response of the system, and the response of the soil foundation obtained by using the proposed approach is neither the free field motion nor the actual foundation input motion. A more rigorous approach would consider the foundation input motion derived from kinematic interaction analysis. However, this paper focuses on the structural response rather than on the SSI effects, which are indeed more complicated than those presented herein.

Advanced and simplified models for HDNR isolators and parameter calibration

The mechanical behaviour of the isolators is described by three different types of models, which are described in the following sections. The first model is an advanced one, recently developed and implemented in OpenSees [39], whilst the other two are described by fewer parameters and thus are considered as simplified models. The latter two models are available in commercial finite-element software and are often employed for the design and analyses of isolated bridges as their use is allowed by current design guidelines under certain design situations (see e.g. [26]).

Advanced HDNR model

The advanced isolator model, denoted hereinafter as HDNR model, has been recently developed and implemented in OpenSees [39] by Kumar et al. [18]. This model consists of a two-node, twelve degrees-of-freedom discrete element. The two nodes are connected by six springs that represent the mechanical behaviour in the six basic directions of the bearing. The HDNR element describes accurately both the nonlinear amplitude-dependent behaviour in shear of the isolator and the vertical behaviour under tensile or compressive loads, as well as the coupling between the responses in different directions. The model input properties are the mechanical parameters required to describe the material behaviour and the geometrical parameters that describe the bearing dimensions.

The shear behaviour of the rubber compound in the horizontal plane is described by the model proposed by Grant et al. [11] for the post-scragged condition. In particular, the relation between the shear force $\mathbf{F}(\mathbf{U})$ and the shear displacement $\mathbf{U}$ is given by the sum of a hyperelastic component $\mathbf{F}_1(\mathbf{U})$ and a hysteretic one $\mathbf{F}_2(\mathbf{U},\mathbf{n})$, depending also on the current direction of the velocity vector $\mathbf{n}$. The hyperelastic response $\mathbf{F}_1(\mathbf{U})$ is given by:

$$\mathbf{F}_1(\mathbf{U}) = \left(a_1 + a_2 \|\mathbf{U}\|^2 + a_3 \|\mathbf{U}\|^4\right)\mathbf{U} \tag{1}$$

whereas the expression for the hysteretic response $\mathbf{F}_2(\mathbf{U},\mathbf{n})$ is controlled by a bounding surface:

$$R(\mathbf{U}) = \left(b_1 + b_2 \|\mathbf{U}\|^2\right) \quad (2)$$

and the rate at which $\mathbf{F}_2(\mathbf{U}, \mathbf{n})$ advances towards the bounding surface upon loading depends on the parameter b_3 [11].

The other values of the material parameters (i.e., c_1, c_2, c_3, c_4) are relevant to the scragging behaviour of the rubber, which is not considered here. Further information regarding the Grant model can be found in [11].

In order to calibrate the parameters for shear behaviour, laboratory tests were carried out at TARRC on double-shear test pieces of HDNR previously scragged at the shear strain amplitude 2.5. In particular, displacement-controlled tests were performed by imposing 20 cycles at increasing strain amplitudes and constant strain rate of 2/s. This rate corresponds to a vibration period between 2 s-3 s for strain amplitudes in the range between 1.0 and 2.0. Fig. 4 compares the experimental hysteretic stable response with the response evaluated by using the HDNR model, at the design strain amplitude of 1.5 (Fig. 4a), and at different amplitudes between 0 and 2.5 (Fig. 4b). The values of the parameters of the Grant et al. [11] model reported in Table 2 have been calibrated to provide the best fit to the experimental results in the range of shear strains between 1 and 1.5. First, the parameters related to the elastic contribution (parameters a_1, a_2 and a_3 of Eqn.(1)) have been fitted by considering the mean relaxed stress–strain line between loading and unloading test results of Fig. 4b. Subsequently, the parameters related to the hysteretic contribution (b_1 and b_2 of Eqn.(2)) have been determined on the basis of Fig. 4a,b. In particular, b_1 has been taken equal to the intercept of the stress-strain curve whereas b_2 has been deducted from the response at large deformations.

Fig. 5 compares the values of the equivalent shear modulus G_{eff} and of the effective damping ratio ξ_{eff} for different values of the shear deformation, according to the test results and to the fitted HDNR model. It can be seen that the HDNR model provides good estimates of both G_{eff} and ξ_{eff}, for $\gamma > 0.5$, whereas for lower shear strains both the shear modulus and the damping are underestimated. This lack of fit is not expected to affect the results, since the design shear deformation is $\gamma_{Ed} = 1.5$.

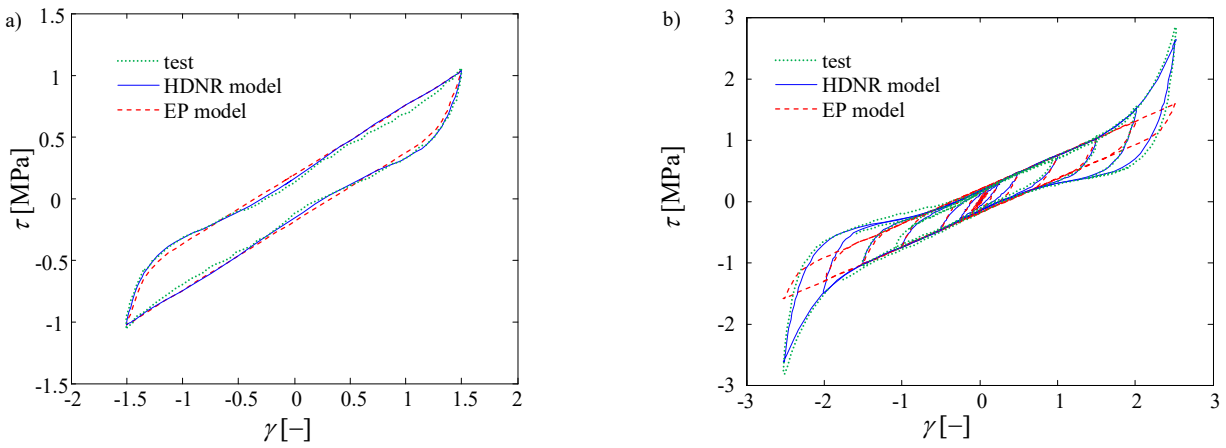

Fig. 4. Stable (20th cycle) hysteretic response according to test results, the HDNR model and to bilinear EP model at (a) the design shear strain amplitude of 1.5, and (b) at different strain amplitudes.

Table 2. Values of Grant et al. model employed for the behaviour in shear.

a_1	a_2	a_3	b_1	b_2	b_3	c_1	c_2	c_3	c_4
kN/m	kN/m^3	kN/m^5	kN	kN/m^2	m^{-1}	m^{-3}	m^{-3}	-	m^{-3}
646.48	-3586.1	24015.7	30.69	402.96	32.65	0	0	1	0

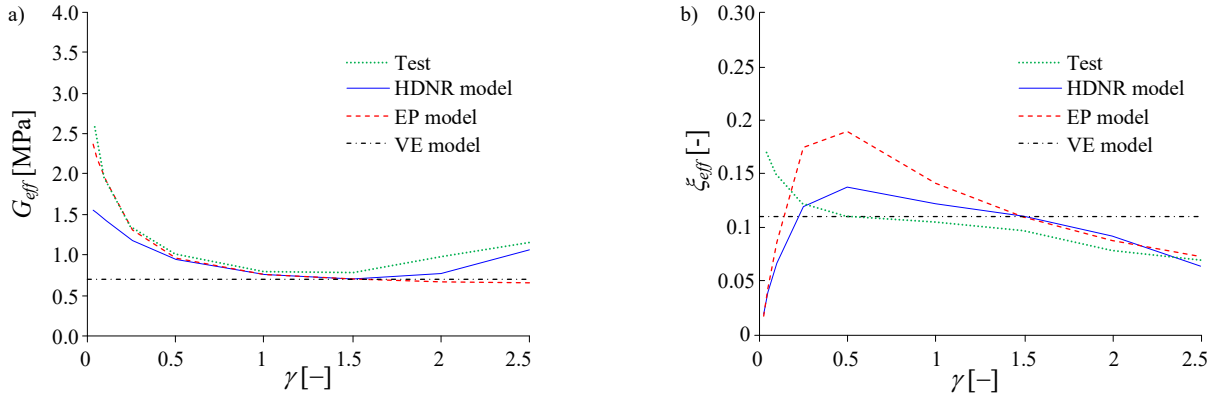

Fig. 5. Variation with maximum shear deformation of equivalent shear modulus (a) and of effective damping ratio (b) of the stable loops.

The horizontal and vertical behaviour of the bearing are coupled due to the following contributions: (1) the dependence of axial stiffness on the magnitude of the lateral displacement, and (2) the variation of shear stiffness with axial load [18]. The axial (i.e. vertical) stiffness K_v of the HDNR model is obtained from the two-spring model of Koh and Kelly [45], which was validated experimentally by Warn et al. [46], and depends strongly on the bearing shape factor S_r through the expression:

$$K_v = K_{v0}\left[1+\frac{3}{\pi^2}\left(\frac{2\|\mathbf{U}\|}{D_r}\right)^2\right]^{-1} \tag{3}$$

where K_{v0} is the initial stiffness at zero displacement, related to S_r.

The shear stiffness decreases for larger values of the compressive axial load that approach the critical buckling load according to the following expression:

$$K_H = K_{H0}\left[1-\left(\frac{P}{P_{cr}^{'}}\right)^2\right] \tag{4}$$

where K_{H0} is initial horizontal stiffness at zero axial load [47][48], P is the axial load, and $P_{cr}^{'}$ is the reduced critical buckling load [18].

The critical buckling load reduces by increasing the shear deformation and its value depends on the effective area of the bearing, i.e., the overlapping area between the top and bottom anchor/bearing plates. Also, the vertical stiffness reduces by increasing the horizontal displacement. It is worth pointing out that the large lateral displacements experienced by the isolators, which correspond to shear strains in the range of 100% - 200%, might lead to substantial reductions in the vertical load-carrying capacity and vertical stiffness of the HDNR bearing [18] [45].

With regard to behaviour of the bearings under tension, prior to the cavitation of the elastomer the vertical stiffness of the steel-laminated rubber bearing is the same as that in compression and it is equal to K_{v0}= 6.22x10^5 kN/m for a single bearing. The onset of cavitation occurs for tensile stresses of the order of $3G$, where G is the shear modulus, and results in a significant stiffness reduction and strength degradation under cyclic loading. The rotational behaviour of the isolators is described by a linear elastic model with rotational stiffness K_r = 5.04x10^3 kN·m/rad for each bearing.

Bilinear hysteretic model

This model, denoted to as elasto-plastic (EP), is a rate-independent hysteretic model, which consists of a nonlinear spring with bi-linear force-displacement relationship describing the behaviour in shear and linear springs simulating the behaviour along the axial and rotational degrees of freedom. The material properties of the bilinear model in shear are evaluated based on the procedure of ASCE 41-13 [29], i.e. by characterising the material properties of the elastomer. In particular, the

data of the 20-th cycle of the characterisation test carried out at the isolator design deformation γ_{is} are used to estimate the equivalent (secant) shear modulus G_{eff} and damping ratio ξ_{eff}. The characteristic strength, i.e., the shear strength at zero strain, τ_0, is obtained as:

$$\tau_0 = \frac{\pi \xi_{eff} G_{eff} \gamma_{is}^2}{\left(2 - \pi \xi_{eff}\right)\gamma_{is} - \gamma_y} \tag{2}$$

where γ_y is the yield strain of the equivalent bilinear model. The value of the post-yielding tangent modulus G_p changes only slightly with the deformation amplitude, and it is assumed such that the maximum stress at γ_{is} is equal to $G_{eff}\gamma_{is}$. The parameters of the EP models considered in the analysis are τ_0 = 0.19 MPa, γ_y =0.1, G_p = 0.56 MPa. A smooth transition between the elastic and post-elastic ranges is assumed. The force-displacement relationship of the spring representing the shear behaviour is then derived by multiplying the stresses by the total rubber area A_r, and the strains by the total rubber height T_r.

The hysteretic stationary response according to the equivalent EP model is plotted also in Fig. 4, together with the responses obtained with the characterisation tests and with the HDNR model. The agreement of the EP an HDNR models at the design strain (Fig. 4a) and at lower strains is very good. However, the EP model cannot describe accurately the increase of stiffness and hysteresis of the rubber for shear strains higher than 1.5 as its post-elastic stiffness is constant.

Fig. 5 shows the variation with the dynamic shear strain amplitude γ_{max} of the equivalent dynamic shear modulus G_{eff} (Fig. 5a) and of the equivalent damping ratio ξ_{eff} (Fig. 5b) according to the HDNR model and to the bilinear model. The agreement is good for the equivalent modulus, with the exception of high amplitudes, for which the EP model is not able to simulate the increase of stiffness, which is mainly due to the strain crystallisation of the rubber. The equivalent damping ratio for the EP model is generally higher than the corresponding ratio for the HDNR model at low amplitudes and very similar at higher amplitudes. The axial and rotational springs of the EP bearing model are assigned a value of the stiffness equal to that of the initial stiffness of the HDNR model.

Visco-elastic model

The visco-elastic (VE) model of the isolators uses linear springs that have the same properties of those of the EP model to simulate the behaviour along the axial and rotational degrees of freedom, and a spring with visco-elastic behaviour to simulate the shear response. The stiffness of the latter spring is evaluated as per Eqn. 3:

$$k_{h,VE} = \frac{G_{eff} A_r}{T_r} \tag{3}$$

where A_r and T_r are the previously defined rubber area and total thickness, and G_{eff} is the secant modulus at the design strain. The value of $k_{h,VE}$ for a single bearing is 751.0 kN/m.

The value of the damper viscous constant c_{VE} is obtained such that the VE model dissipates the same amount of energy of the HDNR model during a closed cycle at the amplitude γ_{is} and at the isolation frequency $\omega_{is} = 2\pi / T_{is}$. This is achieved by assuming:

$$c_{h,VE} = \frac{2 G_{eff} \xi_{eff} A_r}{\omega_{is}} \tag{4}$$

The value of $c_{h,VE}$ assumed in the analyses is 51.63 kN·s/m. Since the VE model is linear, it exhibits no variation of its dynamic properties with the amplitude, as shown in Fig. 5a and Fig. 5b. On the other hand, it should be pointed out that while the behaviour of the HDNR and the EP model is not influenced by the frequency of vibration of motion, the VE model exhibits a significant strain-rate dependency. In fact, the damping ratio $\xi_{VE}(\omega)$ for vibration frequencies ω other than the isolation frequency ω_{is} can be expressed as follows:

$$\xi_{VE}(\omega) = \frac{\xi_{eff} \omega}{\omega_{is}} \tag{5}$$

Thus, the VE model is expected to provide more energy dissipation than the other models for the higher modes of vibration, having frequencies higher than ω_{is} and notably influencing the shear and moment demand of the piers [49].

RESULTS

Following are the results of the analyses investigating in detail the dynamic and seismic behaviour of the benchmark bridge. Emphasis is placed on the effects of the vertical bearing stiffness and on SSI effects on the bridge response. These two effects were found to influence significantly the boundary conditions of the piers. In fact, the eccentrically-placed bearings exert, through their vertical stiffness, a rotational constraint at the pier top, which also depends on the flexibility of the deck and of the continuity slab. A similar effect is observed in the transverse direction for bridges with multiple bearings, also along a single line, and torsionally stiff decks [50]. On the other hand, SSI effects generally involve rocking of the pier base, which may result in an increase of the axial deformation of the bearings.

Fig. 6 illustrates the mechanism involving the coupled horizontal-vertical response of the bearings and the parameters monitored during the seismic analysis that they are used for the assessment of the seismic performance of the isolated bridge. These parameters are:

- the isolator displacements along the horizontal direction ($d_{bh,i}$);
- the isolator compressive and tensile displacements ($d_{bvc,i}$ and $d_{bvt,i}$) and forces ($F_{bvc,i}$ and $F_{bvt,i}$) along the vertical direction;
- the shear and bending moment at the base ($V_{p,base}$ and $M_{p,base}$) and top of the pier ($V_{p,top}$ and $M_{p,top}$);
- the displacements and rotations at the pier top (d_p and r_p);
- the horizontal and vertical displacements of the deck (d_{dh} and d_{dv}).

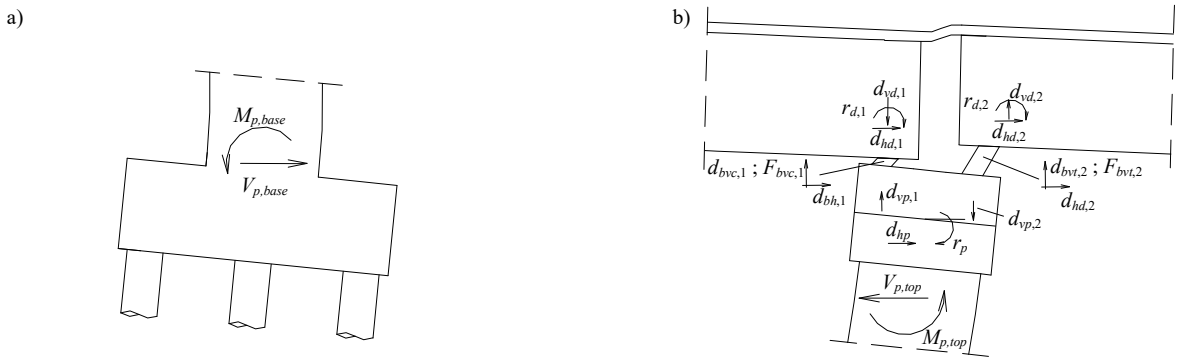

Fig. 6. Mechanism involving the bearing coupled horizontal-vertical response and illustration of monitored response parameters at the pier base (a) and top (b)

Eigenvalue analysis

The eigenvalue analysis of the bridge model is carried out by assuming effective (i.e. secant to the design shear strain) dynamic stiffness properties for the bearing response in shear and the initial stiffness properties (at zero displacement) for the axial behaviour.

Fig. 7 reports the shapes of the most significant vibration modes of the system and Table 3 reports the corresponding modal properties obtained by accounting for SSI effects and by assuming fixed based conditions.

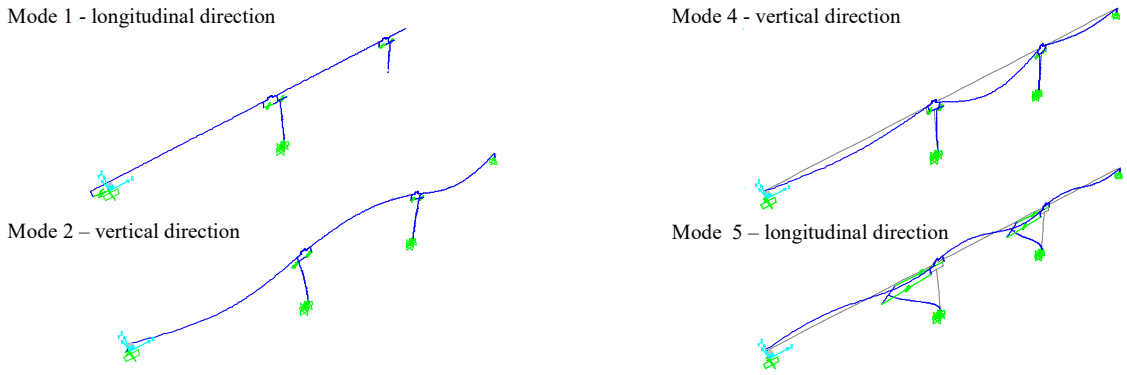

Fig. 7. Modal shapes of the most significant modes of vibration.

Table 3. Periods of vibration and mass participation factors of the most important modes of vibration obtained by considering fixed based conditions and by accounting for SSI effects.

	T [s]		*MPF* [%]	
MODE	Fixed base	SSI	Fixed base	SSI
1	2.023	2.043	78.6	79.5
2	0.281	0.283	17.7	17.4
4	0.252	0.257	47.8	46.6
5	0.125	0.162	10.4	15.2

The first mode of vibration has a period which is very close to the target period of 2.0 s considered for the design. The modal shape is characterised by a significant motion of the deck along the longitudinal direction, whereas the piers do not exhibit significant displacements, since they are isolated. The mode of vibration involving a significant motion of the piers is the 5th one, and its vibration period is relatively small (T = 0.125 s for the fixed-base condition). It is interesting to observe that the horizontal motion of the pier induces a motion of the deck in the vertical direction. This is the result of the pier rotation and of the presence of two eccentric lines of support of bearings over the pier. Modes 2 and 4 characterise the motion of the deck in the vertical direction.

By accounting for SSI effects, the values assumed by the vibration periods remain almost the same, with the exception of mode 5, which increases to 0.162 s. This remarkable increase of vibration period preludes the importance of SSI effects on the response of the piers.

Seismic analysis under horizontal earthquake input

The seismic assessment of the bridge is performed by carrying out non-linear time history analysis of the structure under a set of seven natural records describing the record-to-record variability effects. This ground motion records are selected from the European strong-motion database by using the software Rexel v3.5 [51] and they are compatible with the EC8-1 [25] soil type C spectrum for a PGA of 0.4g. Fig. 8 illustrates the pseudo-acceleration response spectrum of the horizontal and vertical component of the records, obtained for a 5% damping ratio. Further information regarding the records are given in Table 4.

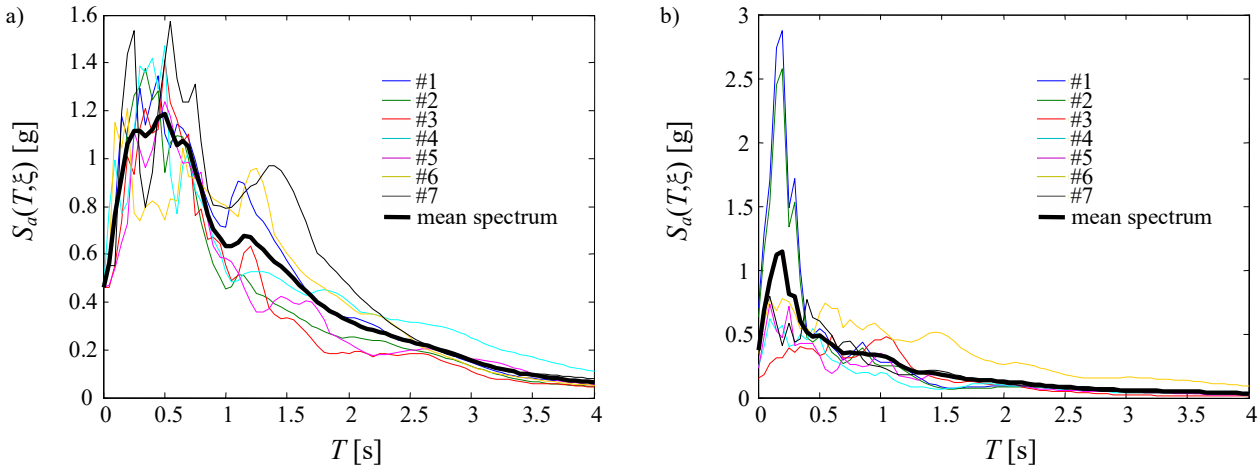

Fig. 8. 5% Pseudo-acceleration spectra of ground motion records and mean spectrum for soil type C spectrum (PGA=0.4g) and 5% damping ratio for the: a) horizontal and the b) vertical component.

Table 4. Characteristics of records employed for the seismic analyses.

#	Name	Station	Earthq. ID	Waveform	Fault	Site class	M_w	R [km]	PGA x [m/s^2]	PGA z [m/s^2]	Scale factor
1	Kalamata	ST164	192	413x	normal	B	5.9	10	2.108	3.250	2.141
2	Kalamata	ST163	192	414x	normal	B	5.9	11	2.354	3.250	1.917
3	Adana	ST549	561	1726y	strike slip	C	6.3	30	2.158	0.866	1.707
4	South Iceland	ST2496	2142	6326y	strike slip	A	6.4	14	1.748	0.610	3.951
5	Alkion	ST121	157	333x	normal	C	6.6	20	2.257	1.138	2.000
6	Campano Lucano	ST93	146	287x	normal	A	6.9	23	1.363	1.017	3.310
7	Montenegro	ST67	93	199y	thrust	B	6.9	16	3.680	2.485	1.269

In order to show the effects of the coupling between the horizontal and vertical response in the

bridge due to the eccentricity of the bearings and SSI effects, the analyses of the reference bridge model are carried out first by considering the horizontal earthquake component only. The time-histories of different response quantities of interest are shown for record #6 of the set of ground motions considered in this study. Fig. 9 shows the time history of the deck displacements and the pier displacements, obtained by accounting for or neglecting the SSI effects, i.e. by assuming a fixed-end foundation.

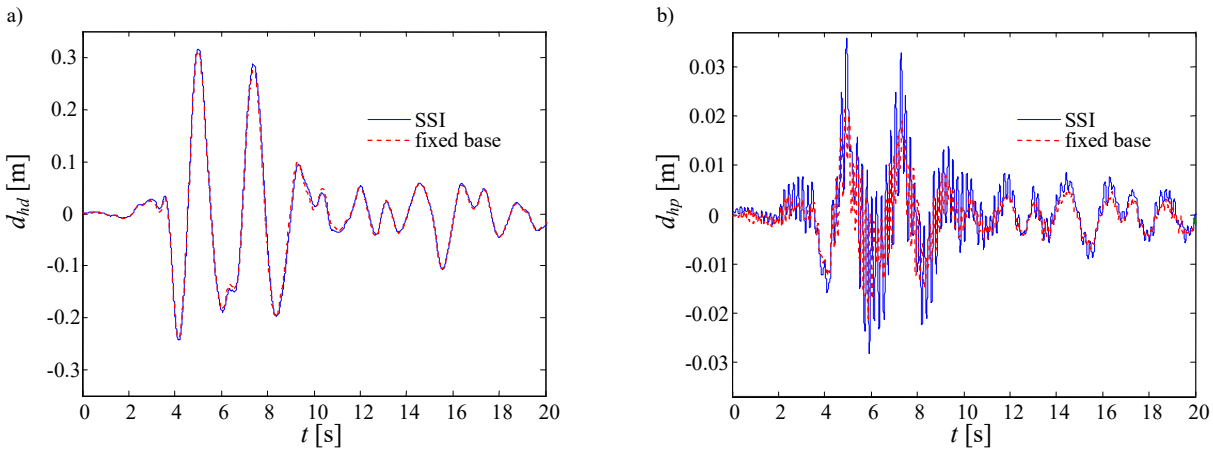

Fig. 9. Time history of the displacement with respect to the ground of (a) the deck and (b) the pier cap obtained by accounting for or disregarding SSI effects for record #6.

The pier displacement response is significantly lower than the deck displacement response, as expected for an isolated bridge. The maximum absolute value of the deck displacement observed for record #6 is about 0.310 m, which is 17% higher than the design value of 0.264 m. Even though the system is characterized by a complex nonlinear behaviour, this difference may be explained by observing in Fig. 8 that record #6 is characterized by a spectral ordinate at the design period which is about 17% higher than the mean spectral ordinate. The scatter between the observed maximum response under the different seismic records and the design record reflects the effect of the so called record-to-record variability, i.e., the differences in the frequency content and duration of the set of records considered for the design, also resulting in the different spectral ordinates of Fig. 8. It is noteworthy that the mean value of the deck displacement, obtained by averaging the results for the seven records, is 0.279 m, i.e. only 6% higher than the design value. In general, the observed deviation from the design value is mainly due to the effects of: the pier flexibility, the nonlinear

447 behaviour of HDNR, the eccentricity of the bearings, and the use of a reduced response spectrum
448 for the design rather than the mean spectrum for the given added damping ratio. The time history of
449 the deck displacement is characterised by a fundamental period of approximately 2.0 s, i.e. the
450 design period, whereas the time history of the pier displacement is characterised by a higher
451 frequency content, since it is influenced by vibration modes of order higher than 1.
452 The SSI effects do not seem to affect significantly the deck displacement demand, whereas they
453 influence significantly the pier demand, as per Fig. 9a and b. In fact, the maximum pier top
454 displacement obtained by accounting for SSI effect (about 0.032 m for record #6) is significantly
455 higher than the corresponding value obtained for the fixed-based condition (about 0.021m). On the
456 other hand, the values of the maximum deck displacement demand, when accounting for or
457 neglecting the SSI effects, are very close to each other i.e. 0.30 m and 0.31 m respectively. For all
458 the cases studied herein, SSI effects cause an increase of the mean pier displacement demand and
459 top rotation. The difference between the pier mean displacement demand obtained by accounting
460 for or disregarding SSI effects, divided by the mean demand obtained by disregarding SSI effects, is
461 about 48%. The corresponding percentage for the pier rotation is 23% and thus the bearing vertical
462 response, which is influenced by the pier rotation, is also dependent on the SSI effects.
463 Fig. 10a shows the time history of the vertical net displacement of the bearings placed on the second
464 line of support, i.e. on the right side of the pier cap. It is remarked that this displacement is the result
465 of the horizontal earthquake excitation, as no vertical input motion has been considered in the
466 analysis. In the same figure, the time history of the product $r_p \cdot e_b$ of the rotation of the pier cap r_p
467 with respect to the y axis times the bearing eccentricity e_b is shown. The two motions are quite
468 different and it is worth to note that the bearing vertical motion depends not only on the pier cap
469 rotation, but also on the vertical displacement of the deck, which is plotted in Fig. 10b. It is also
470 interesting to observe in Fig. 10b that the amplitude of the upwards vertical displacement of the
471 deck induced by the horizontal seismic motion is significantly inferior to the amplitude of the
472 vertical displacement downwards, which increases the compression due to vertical loads. This is the

consequence of the reduction of the vertical stiffness of the bearings under the combination of compression and shear displacements, which is discuss next.

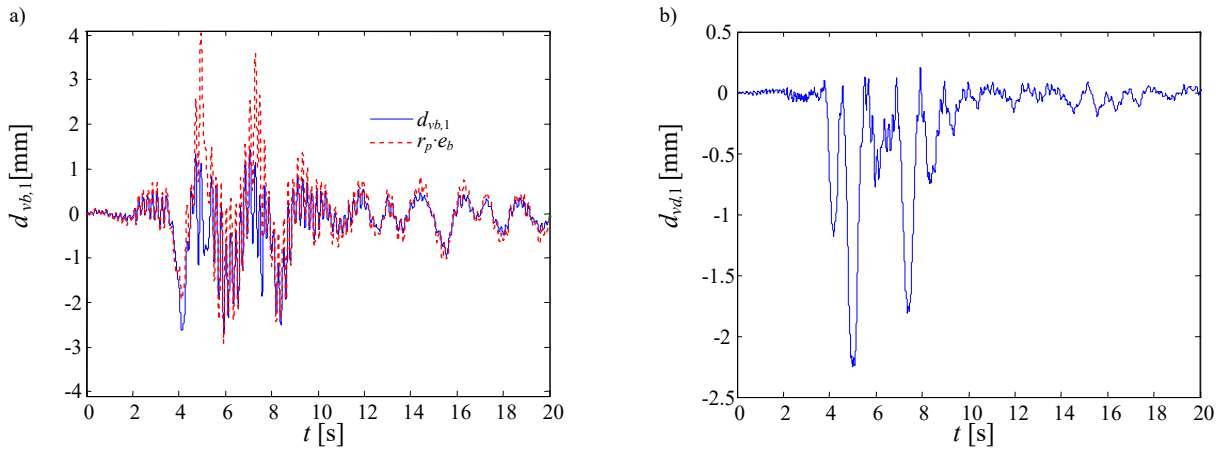

Fig. 10. Time history of (a) the axial deflection of the bearings $d_{vb,1}$ and of the pier rotation times the bearing eccentricity $r_p \cdot e_b$, (b) the deck vertical displacement in correspondence of the second line of bearings over the left pier (record #6).

Fig. 11a and b show the hysteretic response of two bearings placed on the first and second line of support on the pier cap correspondingly, for record #6. The two bearings exhibit similar behaviour in shear (Fig. 11a), with a notable increase of hysteresis for large displacements, i.e. beyond the design one of 0.264 m. Based on Fig. 11b, the vertical response is characterised by a fluctuation of the vertical stiffness, due to the coupling between the horizontal and the vertical response of the isolator. The reduction of the vertical stiffness due to nonlinear geometric effects becomes more significant for large horizontal displacements corresponding to strains larger than 1.5. It is noteworthy that the initial static load on the bearings, due to the self-weight and the additional variable (non-seismic) loads, is 820 kN for the left bearing, and 715 kN for the right bearing, whereas the critical buckling load at zero displacement, calculated based on [47][48], is 4858.7 KN. The critical load reduces to 2757.8 kN at the maximum design displacement of 0.265 m as per the equations provided by Warn et al. [46]. Thus, the values of the vertical loading on the bearings during the time history of the seismic motion are significantly lower than the critical loading value. Moreover, although tensile forces develop within the isolators, the cavitation load of 405.4 kN is not reached in any case examined here. This is due to the fact that the initial static compressive load on the bearings is relatively high and this prevents the development of significant tension and

cavitation of the HDNR bearings.

By calculating the mean value for the seven records considered, SSI effects are found to induce a normalised increase of the bearing vertical displacement demand of about 13% with respect to the fixed-foundation case. This value is significantly inferior to the increase of the pier horizontal deflection demand due to SSI effects (about 48%).

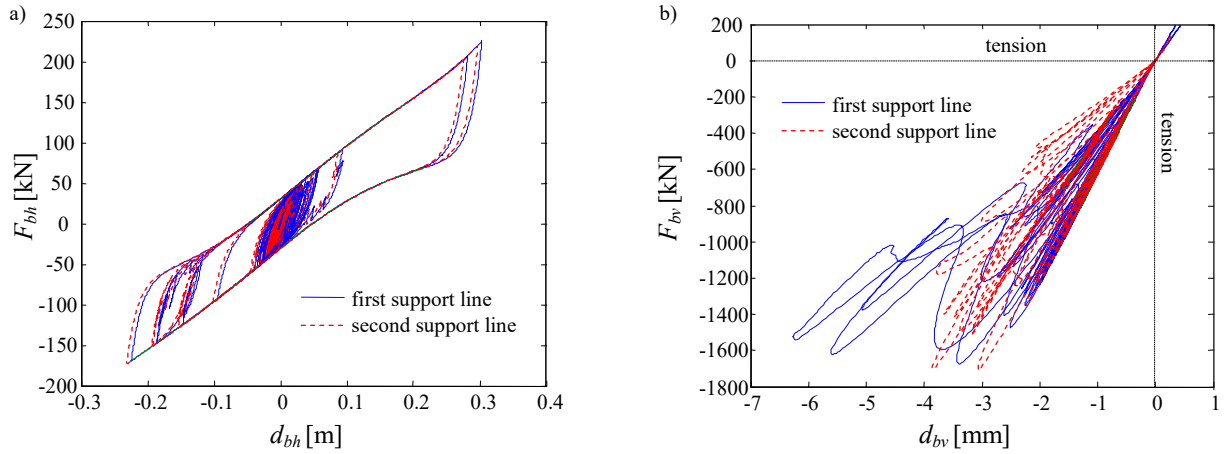

Fig. 11. Response of the bearings in (a) shear and (b) along vertical direction (record #6).

In order to provide further evidence on the fluctuation of the bearing vertical response and the coupling between the horizontal and vertical response of the bridge bearings, the time history of the vertical acceleration of the nodes located on the pier cap below the two lines of bearings is provided in Fig. 12a. These response quantities are denoted respectively as $a_{v,1}$ and $a_{v,2}$, for the first and the second line of support. It can be observed that the time histories of the vertical accelerations measured at the two support lines are in opposition of phase, as they derive from the pier top angular acceleration, which in turn is related to the pier flexure. Thus, their sum, which corresponds to the vertical acceleration at the pier top, is very low. However, the maximum absolute value of $a_{v,2}$, 2.15 m/s^2, is quite high, considering that it is induced solely by the horizontal seismic input and that the vertical seismic component (whose peak value is 3.36 m/s^2) has not been considered in this analysis.

Fig. 12b shows the time history of the vertical acceleration at the base of the pier $a_{pv,\text{base}}$. The maximum acceleration value is non zero because SSI effects have been taken into account. However, it is lower than the value observed at the pier top. Again, this demonstrates that the pier

flexibility and relevant angular rotation increases significantly the vertical motion of the bearings.

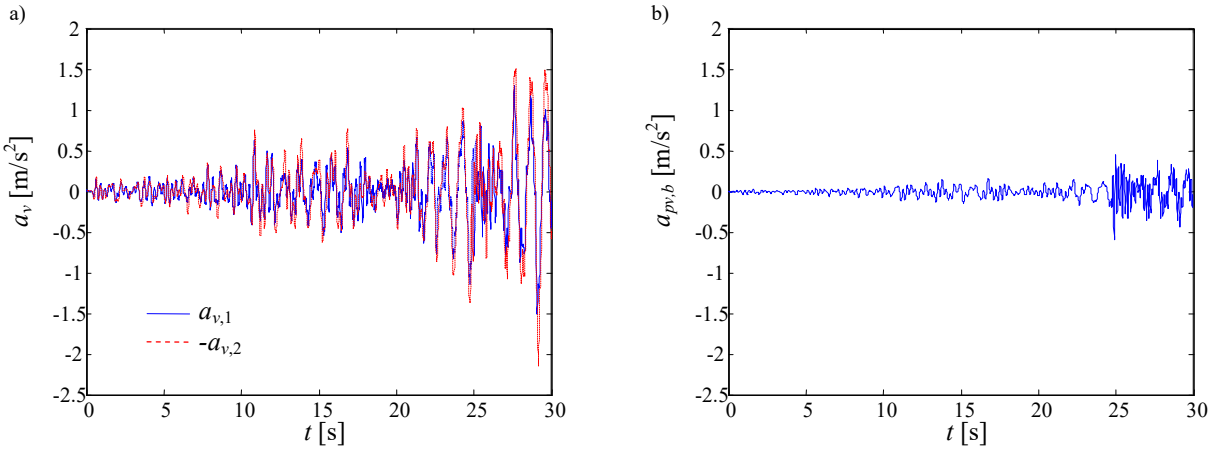

Fig. 12. Time history of the vertical accelerations at the pier top (a) and at the pier base (b) for record #6.

Fig. 13 shows the time history of the bending moment and of the shear force at the base of the pier and at the pier top observed under record #6.

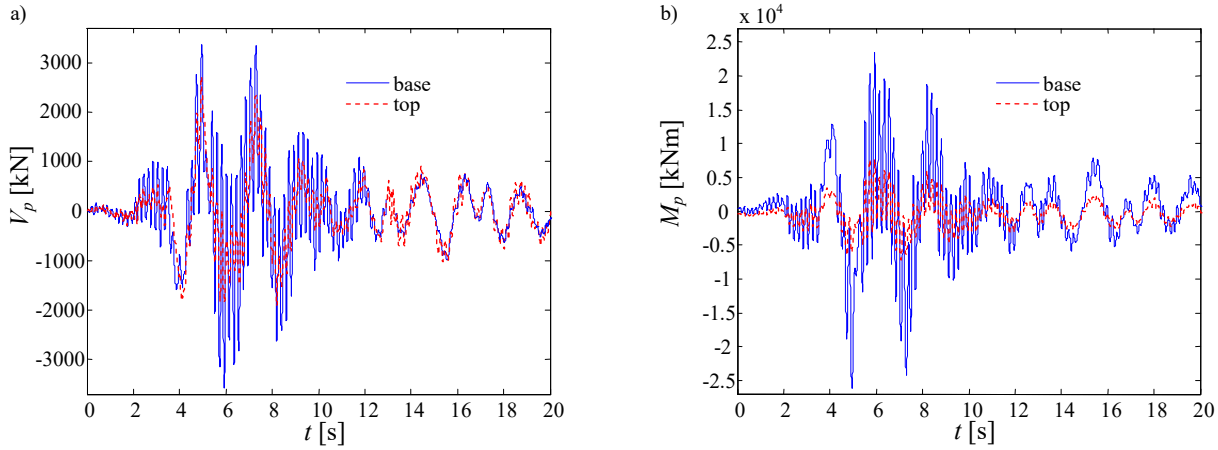

Fig. 13. Time history of the shear force (a) and bending moment (b) at the pier's base and top under record #6.

Unlike the displacement response of the deck, the pier internal actions are significantly influenced by the higher modes of vibrations, which are related to the pier inertia. The ratios between the maximum absolute values of the shear and moment at the top and at the base of the pier are respectively equal to $V_{p,top}/V_{p,base}$ = 0.76 and $M_{p,top}/M_{p,base}$ = 0.35. It is noteworthy that the moment at the pier top is found to be quite significant and it is generated mainly by the couple formed by the axial forces developed within the eccentrically-placed bearings. This is also demonstrated in Fig. 14, showing that the time histories of the moment at the pier top and of the couple formed by the axial forces in the bearings, i.e., ($F_{bv,1}$ - $F_{bv,1}$)e_b, practically coincide.

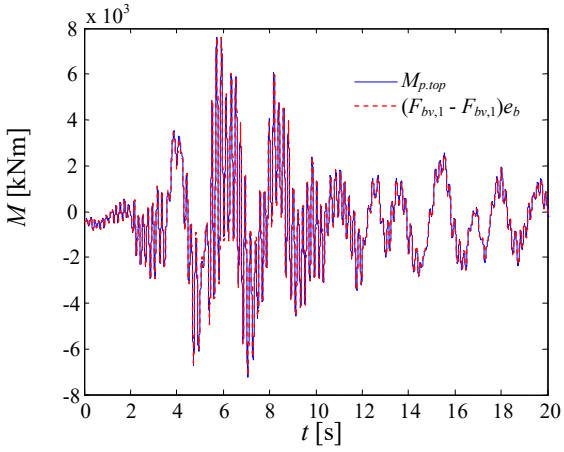

Fig. 14. Time history of the moment at the pier top and of the couple formed by the bearing axial forces.

In the case of a single line of bearings, the pier would behave practically as a cantilever and the moment ratio would be close to zero, as the bending moment at the pier top would be developed only due to the rotational stiffness of the isolators. The moment observed at the pier top in the bridge typology considered is as important as the moment generated at the top of a pier with multiple bearings and torsionally stiff deck in the transverse direction [50], since both these moments could potentially affect the design of the reinforcements and the pier safety evaluation.

Effect the vertical component of the seismic motion

The seismic analyses are repeated by considering the vertical component of the seismic input motion, and the results are compared with the ones previously obtained by considering solely the horizontal component. Fig. 15 shows the time history of the displacement of the deck and of the pier cap obtained by considering the horizontal component of record #6 only and the ones obtained by considering both the horizontal and vertical component. The vertical component of the seismic excitation affects only the time-history of the response of the pier cap d_{hp} (Fig. 15b). However, the maximum values obtained for the two loading cases are approximately the same.

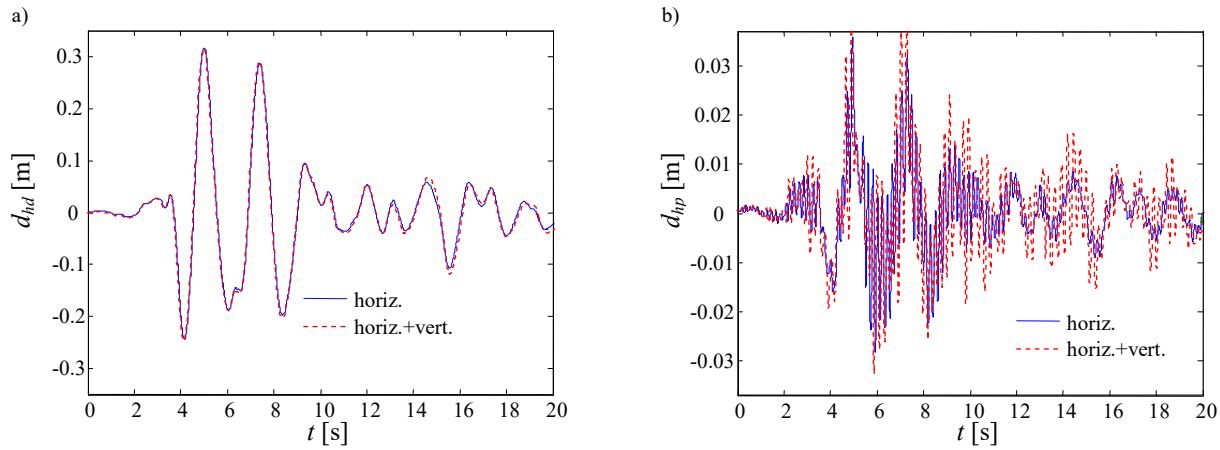

543 Fig. 15. Time history of the displacement with respect to the ground of (a) the deck and (b) the pier cap obtained by
544 accounting for or disregarding the vertical component of the seismic input (record #6).

545 Fig. 16 shows and compares the response of the bearing along the first support line under seismic
546 record #6, obtained by accounting for or disregarding the vertical earthquake component. It can be
547 seen that only the vertical response of the bearings (Fig. 16a) is affected significantly by the vertical
548 excitation. Accounting for it results in higher compressive forces and displacements, inducing
549 significant non-linear geometrical effects, as well as in a higher tensile loads and displacements,
550 beyond the cavitation limit.

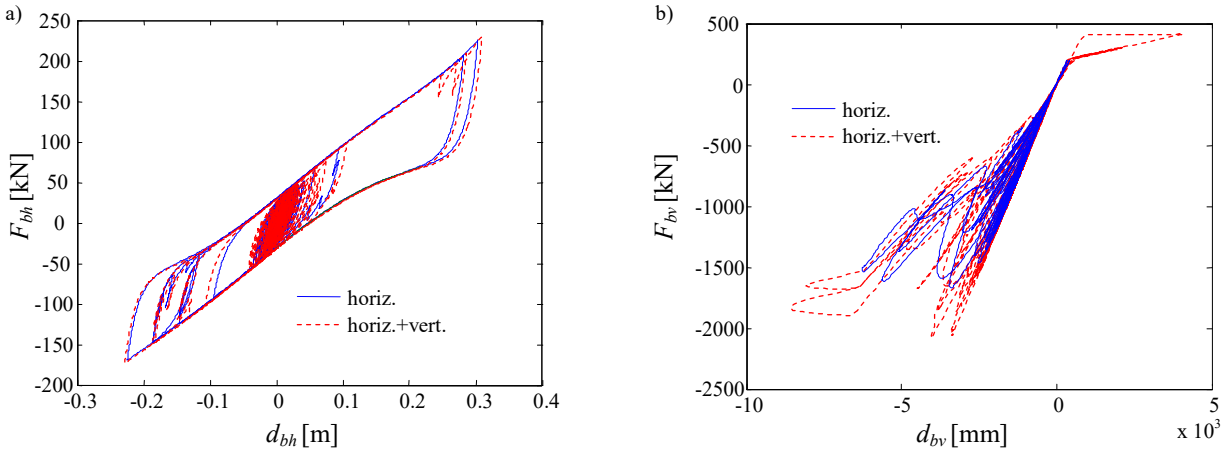

551 Fig. 16. Response of bearing along the first support line in (a) shear and (b) along vertical direction (record #6) obtained
552 by accounting for and by disregarding the vertical component of the seismic input.

553 The maximum values of critical response parameters of the bridge obtained by taking into account
554 or disregarding the vertical excitation of the seismic input are reported Table 5, showing the
555 averaged values for the 7 ground motion records considered.

556

Table 5. Values of the response parameters of interest obtained by considering and by disregarding the vertical component of the seismic input.

Component	horiz	horiz+vert
d_d [m]	0.280	0.278
$d_{bh,1}$ [m]	0.262	0.262
$d_{bh,2}$ [m]	0.258	0.260
d_p [m]	0.031	0.034
r_p [-]	3.60E-03	4.02E-03
$d_{bvt,1}$ [m]	7.79E-05	7.26E-03
$d_{bvt,2}$ [m]	8.34E-05	6.09E-03
$d_{bvc,1}$ [m]	-6.62E-03	-1.07E-02
$d_{bvc,2}$ [m]	-3.98E-03	-8.10E-03
$f_{bvt,1}$ [kN]	33.9	313.1
$f_{bvt,2}$ [kN]	39.6	286.5
$f_{bvc,1}$ [kN]	-1512.3	-2350.8
$f_{bvc,2}$ [kN]	-1440.3	-2134.1
$V_{p,top}$ [kN]	2362.6	2393.3
$V_{p,base}$ [kN]	3003.7	3109.6
$M_{p,top}$ [kNm]	5887.2	6407.8
$M_{p,base}$ [kNm]	22972.5	24582.4

It can be observed that the vertical component of the earthquake input does not affect significantly the horizontal response of the isolators. However, it affects significantly both the maximum compressive and tensile axial loads in the bearings. In particular, the average tensile forces in the bearings increase significantly, even though they do not attain the cavitation limit of 405 kN. Accounting for the vertical component of the seismic input also yields slightly higher values of the internal actions on the pier. In particular, the average bending moment at the pier top increases by 10% due to the vertical component of the seismic input. Generally, it can be said that the vertical component is not expected to affect the design of the piers, but it could influence significantly the dimensioning of the isolators.

Sensitivity of the bridge dynamic response to the vertical isolator stiffness

In order to evaluate the sensitivity of the response of the bridge components to the vertical isolator stiffness, different sets of HDNR isolators are defined that have the same horizontal stiffness, but different values of the shape factor S_r with respect to the reference case discussed in the previous paragraph (S_r = 15). This geometrical parameter denotes the ratio between the loaded area and the force-free area and for a circular bearing of diameter D and thickness of the rubber layer t_r is defined as $S_r = D / 4t_r$. Among other geometrical parameters of the isolators, the shape factor is the parameter that predominantly controls their vertical stiffness. Higher values of the shape factor correspond to greater bearing vertical stiffness and also to larger capacity against buckling. The

number of rubber layers and the single layer thickness are adjusted, whilst keeping unchanged the total rubber thickness and bearing diameter, to maintain the same horizontal stiffness of the bearings of the reference bridge for the different S_r values considered.

The comparison between the design solutions is carried out by assuming the design vibration period T_{is}=2.0 s and the design bearing shear strain of γ_{Ed} =1.5 for all the sets of isolators corresponding to different S_r values, in the range of 10 to 25. This range of shape factors covers the most typical cases of steel-reinforced rubber bearings used in bridge engineering applications. However, it should be noted that for some values of S_r the requirements of design standards may not be satisfied. Fig. 17a shows the variation of the value of the initial vertical stiffness K_{v0} and rotational stiffness K_r of the bearings when the S_r ranges between 10 and 25. These values are normalised with respect to the values corresponding to the reference configuration (corresponding to S_r =15). From this figure it is evident that the increase of K_{v0} and K_r with S_r is significant and follows an almost linear trend. Fig. 17b shows the variation with S_r of the periods of vibration modes 1, 2, 4 and 5, evaluated by accounting for SSI effects, and normalised with respect to the periods corresponding to the reference configuration, i.e. where S_r = 15. The vibration periods reduce only slightly by increasing the shape factor. Higher modes are more affected by the increase of S_r with respect to lower modes. The variation of the modal mass participation factor with S_r, not shown herein due to space constraints, is also not significant.

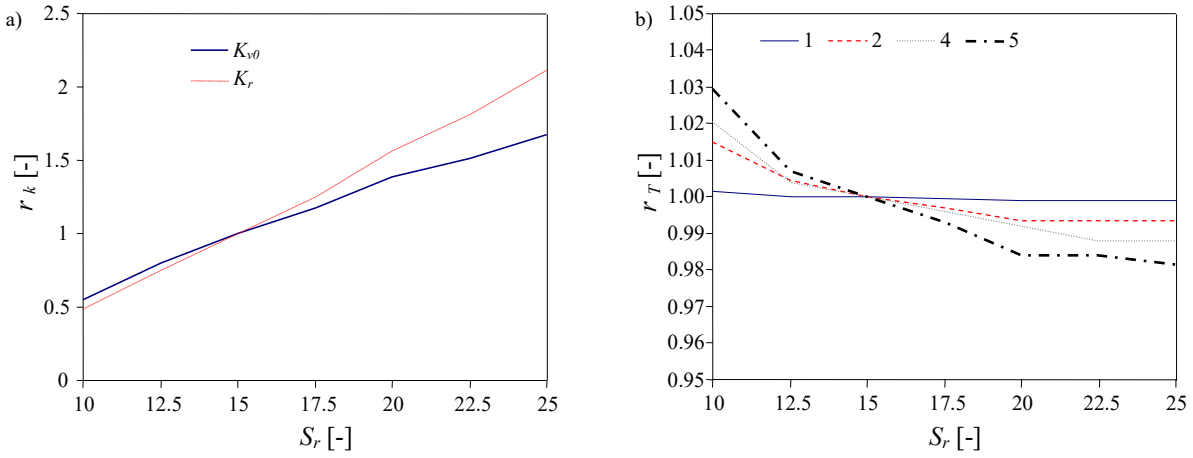

Fig. 17. Variation with S_r of (a) the normalised bearing vertical and rotational stiffness and of (b) the normalised vibration period of the most significant modes.

598 Table 6 reports the maximum values of critical response parameters of the bridge for the different
599 isolation bearings corresponding to shape factors ranging between 10 and 25, obtained by
600 considering both the horizontal and the vertical seismic excitation. It is worth noting that for the
601 seven different analyses shown in Table 1, the bearings have been re-designed, whilst the geometry
602 of the bridge is kept constant, i.e., the pier dimensions and, similarly, the deck section, span length
603 and weight, the continuity slab properties, and the isolator eccentricity are the same as the one of
604 the reference bridge. Additionally, the target design period of the bridge has been kept constant and
605 equal to 2.0 s for all the design cases presented. Hence, the shape factor S_r of the bearings is the
606 only design property that essentially alters the values of the response parameters shown in Table 6.
607 It is observed in Table 6 that the kinematic response quantities related to the pier and deck response
608 are very similar for the different values of S_r. The peak horizontal displacements of the pier and of
609 the deck reduce slightly by increasing S_r. This can be explained by observing that the axial stiffness
610 of the bearings increases when S_r increases. Thus, the rotational restraint at the pier top that is
611 provided by the eccentrically-placed bearings increases for larger S_r values and this reduces the
612 seismic demand at the piers top.
613 On the other hand, the absolute values of the compressive and tensile forces in the bearings alter
614 significantly with S_r. They first decrease, then they increase again, the minimum values
615 corresponding to S_r=12.5. This trend is the result of the complex dynamic behaviour of the system,
616 which is characterised by a contribution to the bearing forces due to the vertical static loads acting
617 on the deck, the pier rotation, and the motion of the deck in the vertical direction. It is noteworthy
618 that the peak tensile forces values for all the S_r values are always inferior to the force that causes
619 cavitation, i.e. 405 kN.
620
621
622
623

Table 6. Values of the response parameters of interest corresponding to different values of the shape factor (S_r)*

S_r	10	12.5	15	17.5	20	22.5	25
d_d [m]	0.279	0.278	0.278	0.277	0.277	0.277	0.276
$d_{bh,1}$ [m]	0.260	0.261	0.262	0.262	0.263	0.263	0.264
$d_{bh,2}$ [m]	0.257	0.259	0.260	0.262	0.263	0.263	0.264
d_p [m]	0.035	0.034	0.034	0.034	0.033	0.033	0.033
r_p [rad]	4.27E-03	4.11E-03	4.02E-03	3.94E-03	3.74E-03	3.66E-03	3.65E-03
$d_{bvt,1}$ [m]	2.36E-02	6.01E-03	7.26E-03	7.56E-03	7.93E-03	8.25E-03	8.47E-03
$d_{bvt,2}$ [m]	2.36E-02	4.96E-03	6.09E-03	6.51E-03	7.42E-03	7.61E-03	7.92E-03
$d_{bvc,1}$ [m]	-3.56E-02	-1.36E-02	-1.07E-02	-8.95E-03	-6.71E-03	-5.80E-03	-4.93E-03
$d_{bvc,2}$ [m]	-3.42E-02	-1.07E-02	-8.10E-03	-6.49E-03	-4.76E-03	-4.14E-03	-3.66E-03
$f_{bvt,1}$ [kN]	287.1	260.4	313.1	327.2	336.5	340.7	344.5
$f_{bvt,2}$ [kN]	315.4	237.6	286.5	320.4	347.9	362.2	377.3
$f_{bvc,1}$ [kN]	-2317.9	-1986.9	-2350.8	-2457.2	-2580.3	-2638.7	-2739.4
$f_{bvc,2}$ [kN]	-2079.8	-1901.0	-2134.1	-2177.4	-2345.1	-2422.6	-2429.5
$V_{p,top}$ [kN]	2332.0	2338.5	2393.3	2471.1	2483.3	2467.1	2498.5
$V_{p,base}$ [kN]	2912.4	3038.6	3109.6	3355.9	3465.5	3447.6	3416.2
$M_{p,top}$ [kNm]	5490.2	5628.8	6407.8	6815.2	7310.1	7565.8	7875.5
$M_{p,base}$ [kNm]	24864.2	24426.7	24582.4	24991.8	25034.6	24764.9	24540.8

With regard to pier internal actions, the shear demand along the pier is not significantly affected by the bearing shape factor, since it mainly depends on the force transmitted by the bearings (which does not alter significantly when varying the value of S_r), and to a minor extent on the higher modes of vibration related to the pier inertia. On the other hand, the moment demand at the pier top increases significantly by increasing S_r, as a result of the increase of the rotational restraint at the pier top. In fact, for S_r = 10, which represents bearings that are relatively flexible axially, the ratio between the pier top and base bending moment is equal to 0.22, whereas for S_r=25, corresponding to stiffer bearings, this ratio is 0.32. This indicates that the stiffer the bearing axially, the more the pier top is fixed, i.e. the more the pier response deviates from that of a cantilever. This result is potentially important because in design practice lower amount of reinforcement is usually provided at the pier top than at the pier base, assuming that the pier behaves as a cantilever, which is not accurate either.

Evaluation of the accuracy of the simplified bearing models

The results of the analyses of the benchmark bridge discussed above show that the accurate modelling of the bearings and in particular of their vertical stiffness influences significantly the dynamic response of the system. Hence, it is important to define the level of accuracy that is

642 achieved when employing simplified bearing models for the design and assessment of bridges. For
643 this purpose, the analysis of the reference bridge model considered above is repeated by replacing
644 the advanced bearing model with the simplified elasto-plastic (EP) and visco-elastic (VE) models,
645 which have uncoupled axial and shear behaviour. It is noted that these models considering an EP
646 and VE behaviour for the bearings are still characterized by the bearings placed eccentrically, i.e. as
647 in the case of the HDNR model. A comparison is made between the response estimates obtained by
648 using the different bearing models, and the corresponding estimates obtained by using the more
649 advanced and accurate HDNR bearing model. Along with the bridge models with eccentrically
650 placed bearings, a simplified and practice-oriented SDOF model of the bridge is considered, the
651 properties of which are derived by assuming that the pier behaves as a cantilever, and that the
652 bearings, described by the VE model, are simply placed at the pier top with no eccentricity. Under
653 these assumptions, the stiffness of the SDOF system can be found based on a series arrangement of
654 two visco-elastic systems, representing respectively the pier and the bearing [49]. In particular, the
655 stiffness of the spring related to the pier is taken equal to $3EI_p / h_p^3$, where EI_p is the cracked pier
656 flexural rigidity, and h_p is the pier height. The mass of the system on the other hand can be taken as
657 the deck tributary mass. The corresponding bridge model, hereafter referred to as VE-SDOF model,
658 is widely employed in design practice for a preliminary evaluation of the isolated bridge response
659 based on simple calculations involving the use of a response spectrum and a damping reduction
660 factor (see e.g.[26]).
661 The results reported in Fig. 18 to Fig. 21, showing the time history of the most important response
662 parameter of interest according to the different bridge and bearing models, have been obtained by
663 considering the horizontal earthquake input only. However, in the final part of the section the
664 evaluation of the accuracy of the simplified isolator models is carried out by considering also the
665 vertical component. Fig. 18 shows the time history of the horizontal displacements of the deck
666 according to the two simplified models. The corresponding time histories obtained using the HDNR

667 model are also shown for comparison.

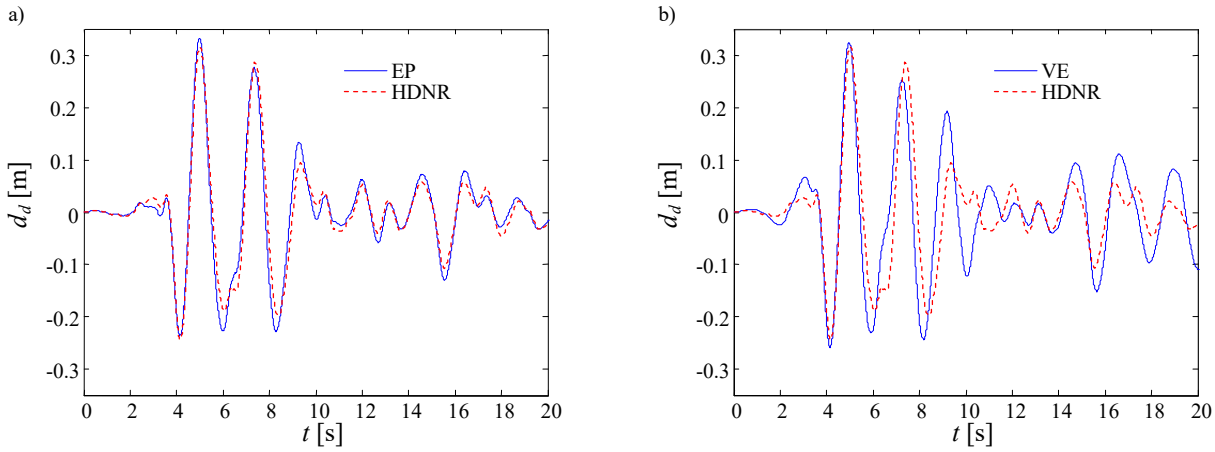

668 Fig. 18. Time history of the displacement of the deck obtained by considering the EP bearing model (a) and the VE
669 bearing model (b) under record #6.

670 The two simplified models provide estimates of the peak deck displacements similar to the ones
671 obtained by using the HDNR bearing model. This can be explained by observing that these response
672 quantities are mainly governed by the first mode of vibration of the system and at the design
673 isolation frequency and displacement amplitude the HDNR, the EP, VE and HDNR bearing models
674 are characterised by similar equivalent stiffness and damping properties, as shown in Fig. 5. It is
675 also worth noting that during the time interval 4s to 8s, where the maximum displacements are
676 attained, the oscillation period of the motion is very close to the design period of 2.0 s.
677 Fig. 19 shows the time history of the displacement of the pier top for the simplified models
678 subjected to record #6. While the EP model provides values of the displacements similar to the ones
679 obtained by the HDNR model, the VE model yields smaller values. This is due to the fact that both
680 the HDNR and the EP model are rate-independent models, whereas the VE exhibits a significant
681 rate-dependency which results in an overestimation of the damping for vibration frequencies higher
682 than the design one (see Eqn. (5)). Thus, the contribution of higher modes of vibration, which are
683 known to affect significantly the pier response ([49]), is damped out by using the VE model.

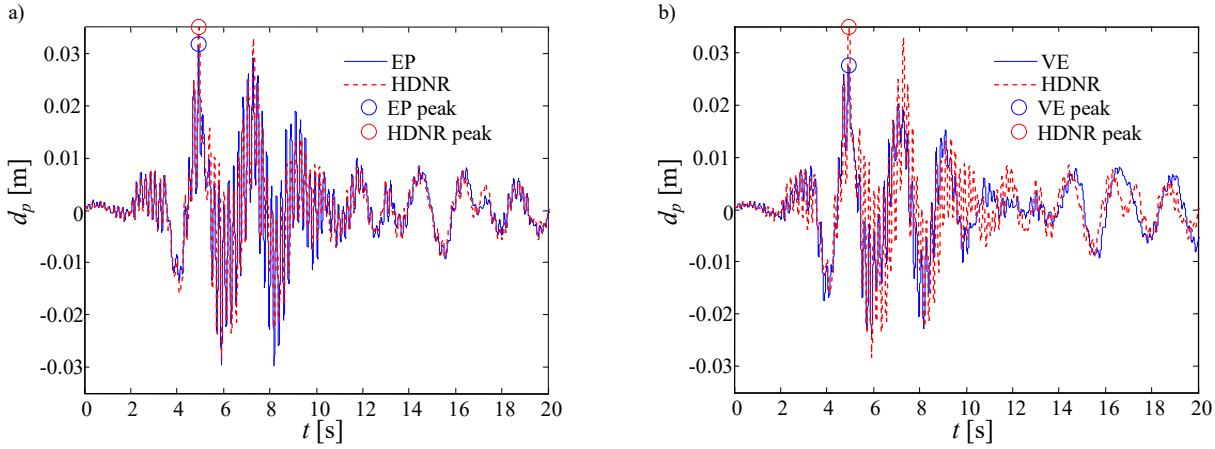

Fig. 19. Time history of the displacement of the pier top obtained by considering the EP bearing model (a) and the VE bearing model (b) under record #6.

Fig. 20 and Fig. 21 show the time history of respectively the base shear and bending moment of the piers when to the two simplified models were employed. These time histories are compared with the ones obtained by using the HDNR model, which are reported in Fig. 13. The results show that the VE bearing model underestimates the values of V_p and of M_p with respect to the HDNR bearing model, as higher modes contribution are damped out.

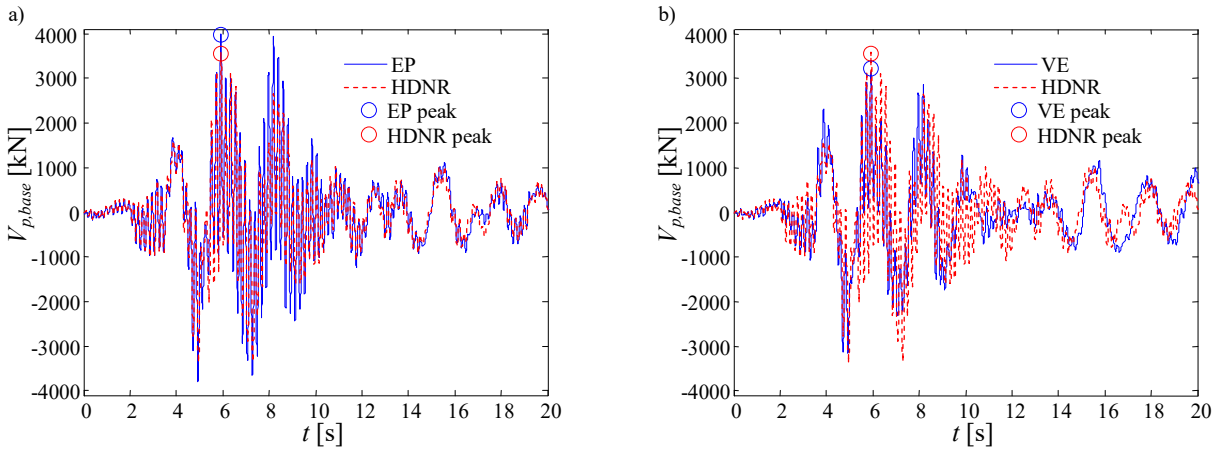

Fig. 20. Shear force at the base of the pier obtained by employing the EP bearing model (a) and the VE bearing model (b) under record #6.

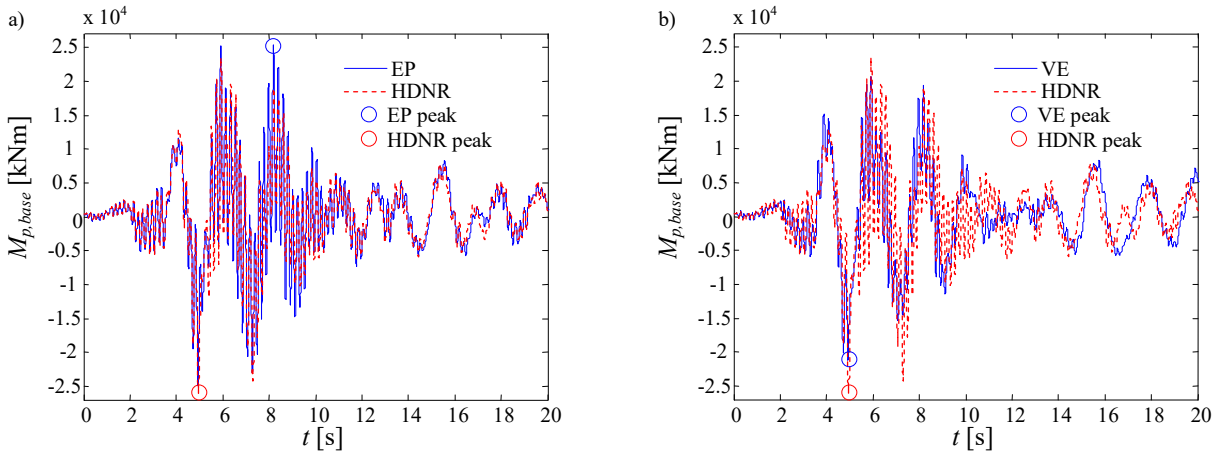

Fig. 21. Bending moment at the base of the pier obtained by employing the EP bearing model (a) and the VE bearing model (b) under record #6.

Table 7 reports the mean peak values of the responses of the bridge components for the different models employed in the analysis, obtained by considering either the horizontal component only, or both the horizontal and vertical component.

Table 7. Comparison of the estimates of the peak response according to the different bridge and isolators models.

	Horizontal component only				Horizontal + vertical component			
	HDNR	EP	VE	VE –SDOF	HDNR	EP	VE	VE -SDOF
d_d [m]	0.280	0.298	0.275	0.263	0.278	0.295	0.275	0.263
$d_{bh,1}$ [m]	0.262	0.288	0.262	0.237	0.262	0.289	0.265	0.237
$d_{bh,2}$ [m]	0.258	0.284	0.259	0.237	0.260	0.290	0.265	0.237
d_p [m]	0.031	0.026	0.022	0.026	0.034	0.032	0.027	0.026
r_p [rad]	3.60E-03	2.58E-03	2.25E-03	3.48E-03	4.02E-03	3.40E-03	2.80E-03	3.48E-03
$d_{bvt,1}$ [m]	0.779E-04	3.31E-04	1.65E-04	3.94E-04	7.26E-03	1.30E-03	1.10E-03	3.94E-04
$d_{bvt,2}$ [m]	8.34E-05	6.45E-04	4.46E-04	3.94E-04	6.09E-03	1.10E-03	9.16E-04	3.94E-04
$d_{bvc,1}$ [m]	-6.62E-03	-3.11E-03	-2.87E-03	-2.39E-03	-1.07E-02	-3.80E-03	-3.50E-03	-2.39E-03
$d_{bvc,2}$ [m]	-3.98E-03	-2.65E-03	-2.46E-03	-2.39E-03	-8.10E-03	-3.30E-03	-3.00E-03	-2.39E-03
$F_{bvt,1}$ [kN]	33.9	205.6	102.4	244.8	313.1	808.9	686.7	244.8
$F_{bvt,2}$ [kN]	39.6	401.3	277.5	244.8	286.5	699.6	569.8	244.8
$F_{bvc,1}$ [kN]	-1512.3	-1936.2	-1786.2	-1488.3	-2350.8	-2357.7	-2194.7	-1488.3
$F_{bvc,2}$ [kN]	-1440.3	-1648.9	-1529.8	-1488.3	-2134.1	-2051.2	-1874.0	-1488.3
$V_{p,top}$ [kN]	2362.6	2421.5	2293.1	2137.3	2393.3	2535.0	2418.3	2137.3
$V_{p,base}$ [kN]	3003.7	3166.2	2679.8	2137.3	3109.6	3599.5	2999.9	2137.3
$M_{p,top}$ [kNm]	5887.2	9103.2	7885.0	0	6407.8	9057.5	8358.2	0
$M_{p,base}$ [kNm]	22972.5	20364.1	17570.6	21372.8	24582.4	24485.0	20554.0	21372.8

Similar conclusions can be drawn for the two different loading scenarios. With regard to

displacement demand of the deck, the piers and the isolators all the models provide similar estimates. The EP slightly overestimates these demands, whereas the VE model provides values closer to the ones obtained by using the HDNR model. The VE-SDOF model, despite being a simplified one, provides a reasonably good estimate of the deck displacement demand, but underestimates the displacement demand of the bearings. This is due to the fact that this model neglects the contribution of higher modes of vibration and employs a reduced response spectrum to obtain an estimate of the seismic displacement, while accounting for the isolators damping.

The values of the peak pier top rotation estimated using the simplified EP and VE models are significantly lower than the values obtained based on the advanced bearing model. This is the consequence of the fact that the simplified models do not account for the reduction of bearing axial stiffness and thus neglect the rotational restraint at the pier head, during the earthquake (Fig. 11b). For the same reason, the estimates of the bearing axial forces based on the simplified models are not accurate. This aspect is critical as the simplified models overestimate the tensile forces within the isolator and this may lead to the incorrect conclusion that the bearings might experience cavitation. However, it should be pointed out that simplified models provide conservative estimates of the tensile forces, whereas the absolute value of the compressive forces is on the other hand underestimated as nonlinear geometrical effects are disregarded.

The rotation of the top of the piers according to the simplified VE-SDOF model is higher since the piers are assumed to behave as cantilevers, i.e. no rotational restraints are assumed at their head. The shear demand estimates based on the EP model are higher than the corresponding ones evaluated by using the HDNR model, whereas that estimates according to the VE model are not conservative, because of the underestimation of the contribution of higher modes. Similar observations hold for the bending moment demand at the pier base, whereas with reference to the bending moment demand at the pier top, both the EP and VE provide conservative estimates as compared to the estimates obtained with the advanced model. This is the result of the fact that this response quantity is influenced by the rotational restraint at the pier top, which is controlled by the

axial bearing stiffness. This stiffness is assumed constant in the case of the simplified models and it is always greater or equal to the corresponding stiffness of the advanced bearing model, which accounts for the coupling between the horizontal and vertical response. As expected, the estimates of the pier internal actions obtained by considering the VE-SDOF model of the bridge are in general quite inaccurate, with the exception of the pier base moment. The peak value of this response quantity is very similar to that of the reference model, even though it is evaluated under the assumption that the pier behaves as a cantilever.

CONCLUSIONS

This paper investigated the accuracy of simplified bearing models for the analysis of the seismic response of multi-span simply supported (MSSS) bridges isolated with steel-reinforced HDNR bearings. MSSS bridges are characterised by bearings placed eccentrically with respect to the pier axis, which introduces a strong coupling of the horizontal and the vertical response of the system. Recently, advanced models were made available for describing the bearing behaviour and this has offered the opportunity to better understand the response of MSSS bridges and to evaluate the accuracy of simplified bearing models for the seismic response assessment.

A benchmark three-span bridge, representative of many isolated bridges erected in Europe, was considered for this study and the following conclusions were drawn by employing the advanced bearing model in the evaluation of the response to a set of ground motion records:

- Significant fluctuations of the axial forces of the bearing were observed, even when only the horizontal component of the earthquake excitation is considered. In particular, the pier top rotations contribute toward significant axial deformations of the bearings, which may induce tension or buckling under certain design situations.
- The isolated piers do not behave as cantilevers under horizontal seismic excitations due to the fact that the isolators partially restrain the rotation of the pier top. As a result, the pier response may be similar to that of a column clamped at the base with partial restraint at its top.

752 -The SSI effects, inducing rotations at the pier base, influence significantly the horizontal
753 displacement and rotation demand at the pier top and thus should be considered in the analysis of
754 MSSS bridges. For the analysed benchmark bridge, the mean pier horizontal deflection demand
755 under the longitudinal earthquake input increases by 48% due to SSI effects, whereas the bearing
756 vertical displacement demand by about 13% with respected to the fixed-foundation case.
757 - The vertical component of the earthquake input motion does not affect significantly the horizontal
758 response of the isolators and the horizontal displacements of the deck. However, it affects
759 significantly both the maximum compressive and tensile axial loads within the bearings, and to a
760 lesser extent the internal actions in the piers.
761 - The sensitivity study carried out to evaluate the influence of the vertical stiffness of the bearings
762 on the dynamic response of the bridge showed that the periods of the most significant modes of
763 vibration are slightly affected by the variations of the shape factor S_r. However, the bending
764 moment at the pier top, the shear forces in the pier, and the axial forces of the bearings are strongly
765 dependent on the shape factor S_r. In particular, the bending moment and the shear demands increase
766 for larger values of S_r due to the stronger rotational restraint at the pier top, which in turn is
767 controlled by the axial stiffness of the eccentrically placed bearings. With regard to bearing
768 compressive and tensile forces, their absolute value first decreases, when S_r ranges between 10 and
769 12.5, and then increases again, when S_r has values larger than 12.5. This is the result of two
770 counteracting effects, i.e., the increase of axial stiffness and the reduction of rotational demand for
771 increasing S_r values.
772 The evaluation of the accuracy and reliability of two simplified bearing models, which are widely
773 used in design practice, was also examined. The simplified models were assumed to have either
774 elasto-plastic (EP) and visco-elastic (VE) behaviour in shear, but with a constant axial bearing
775 stiffness throughout the analyses. The estimates of the pier and deck displacement demand obtained
776 by the simplified models are quite accurate and similar to the estimates obtained by using the
777 advanced bearing model. This is mainly due to the fact that the simplified models provide the same

778 level of damping and stiffness of the advanced model for the design vibration frequency and
779 amplitude. However, the estimates of other parameters relevant to the bridge performance, such as
780 the pier bending moments and shear forces, were found to be not accurate. In particular, the EP and
781 the VE model provide respectively conservative and generally non-conservative estimates of these
782 quantities compared to the accurate HDNR bearing model. This is the consequence of the
783 contribution of the higher modes of vibration to the response and the different behaviour of the
784 simplified models with respect to the advanced models both in terms of horizontal stiffness and
785 damping and of axial stiffness. In particular, it was found that the estimates of the internal actions
786 according to the VE model are not conservative because the contribution of higher modes of
787 vibration is damped excessively.
788 With reference to the estimates of the bearing response, both the simplified models yield absolute
789 values of the compressive and tensile forces higher than the corresponding values obtained with the
790 advanced bearing model.
791 Future studies should address the influence of the transverse horizontal component of the seismic
792 excitation on the bridge and bearing response prediction and the accuracy of the equivalent models
793 for seismic intensities other than the design one and for earthquake inputs of different
794 characteristics and/or including pulses. It is noteworthy that the results presented in the paper have
795 been obtained by considering a simplified approach for the soil-structure interaction analysis. Thus,
796 a more detailed analysis of the bridge-soil-foundation system accounting for the seismic input
797 according to kinematic analysis and including the rocking motion at the foundation level will also
798 be considered in future studies.

799 # REFERENCES

800 [1] Lee GC, Kitane Y, Buckle IG. Literature review of the observed performance of seismically
801 isolated bridges. Research Progress and Accomplishments: Multidisciplinary Center for
802 Earthquake Engineering Research 2001; 51-62.
803 [2] Chaudhary MTA, Abe M, Fujino Y. Performance evaluation of base-isolated Yama-ag´e
804 bridge with high damping rubber bearings using recorded seismic data. Engineering
805 Structures 2001; 23(8): 902-910.

[3] Boroschek RL, Moroni MO, Sarrazin M. Dynamic characteristics of a long span seismic isolated bridge. Engineering Structures 2003; 25 (12): 1479-1490.
[4] Shen J., Tsai MH, Chang KC, Lee GC. Performance of a seismically isolated bridge under near-fault earthquake ground motions. Journal of Structural Engineering 2004; 130 (6): 861-868.
[5] Sarrazin M, Moroni O, Roesset JM. Evaluation of dynamic response characteristics of seismically isolated bridges in Chile. Earthquake Engineering & Structural Dynamics 2005; 34(4-5): 425–448.
[6] Fuller KNG, Gough J, Pond TJ, Ahmadi HR. High damping natural rubber seismic isolators. J. Struct. Control 1997; 4 (2): 19-40.
[7] Ahmadi HR, Kingston JGR, Muhr AH. Dynamic Properties of Filled Rubber - Part I: Simple Model, Experimental Data and Simulated Results. Rubber Chemistry and Technology 2008; 81 (1): 1-18.
[8] Tubaldi E, Ragni L, Dall'Asta A, Ahmadi H, Muhr A. Stress softening behaviour of HDNR bearings: modelling and influence on the seismic response of isolated structures. Earthquake Engineering &Structural Dynamics 2017; 10.1002/eqe.2897.
[9] Huang WH. Bi-Directional Testing, Modeling, and System Response of Seismically Isolated Bridges. Ph. D. thesis, 2002; University of California, Berkeley.
[10] Abe M, Yoshida J, Fujino Y. Multiaxial Behaviours of Laminated Rubber Bearings and their Modeling. II:Modelling. Journal of Structural Engineering 2004, 130 (8): 1133-1144.
[11] Grant DN, Fenves GL, Auricchio F. Modelling and analysis of High damping Rubber Bearings for the seismic protection of bridges. Iuss Press: Pavia, 2005.
[12] Ryan K, Chopra A. Estimating Seismic Demands for Isolation Bearings with Building Overturning Effects. Journal of Structural Engineering 2006; 132 (7): 1118-1128.
[13] Katsaras CP, Panagiotakos TB, Kolias B. Effect of torsional stiffness of prestressed concrete box girders and uplift of abutment bearings on seismic performance of bridges. Bulletin of Earthquake Engineering 2009; 7 (2), 363-375.
[14] Mitoulis SA. Uplift of elastomeric bearings in isolated bridges subjected to longitudinal seismic excitations. Structure and Infrastructure Engineering: Maintenance, Management, Life-Cycle Design and Performance 2015; 11 (12): 1600-1615.
[15] Tubaldi E, Mitoulis SA, Ahmadi H, Muhr A. A parametric study on the axial behaviour of elastomeric isolators in multi-span bridges subjected to horizontal seismic excitations. Bulletin of Earthquake Engineering 2016; 14 (4): 1285-1310.
[16] Gent AN. Cavitation in rubber: a cautionary tale. Rubber Chemistry Technology 1990; 63 (3): 49–53.
[17] Dorfmann A, Burtscher SL. Aspects of cavitation damage in seismic bearings. Journal of Structural Engineering 2000; 126 (5): 573-579.
[18] Kumar M, Whittaker AS, Constantinou MC. An advanced numerical model of elastomeric seismic isolation bearings. Earthquake Engineering & Structural Dynamics 2014; 43 (13): 1955-1974.
[19] Cardone D, Perrone G. Critical load of slender elastomeric seismic isolators: an experimental perspective. Engineering Structures 2012; 40, 198-204.
[20] Siqueira GH, Tavares DH, Paultre P, Padgett JE. Performance evaluation of natural rubber seismic isolators as a retrofit measure for typical multi-span concrete bridges in eastern Canada. Engineering Structures 2014; 74: 300-310.
[21] Cardone D, Dolce M, Palermo G. Direct displacement-based design of seismically isolated bridges. Bulletin of Earthquake Engineering 2009; 7(2): 391-410.
[22] Jara JM, Villanueva D, Jara M, Olmos B. A. Isolation parameters for improving the seismic performance of irregular bridges. Bulletin of Earthquake Engineering 2013;11(2): 663-686.

[23] Zanardo G, Hao H, Modena C. Seismic response of multi‐span simply supported bridges to a spatially varying earthquake ground motion. Earthquake Engineering & Structural Dynamics 2002; 31 (6): 1325-1345.
[24] Matsagar VA, Jangid RS. Seismic response of simply supported base-isolated bridge with different isolators. International Journal of Applied Science and Engineering 2006; 4(1): 53-69.
[25] EN 1998-1. Eurocode 8: Design of structures for earthquake resistance, Part 1: General rules, seismic actions and rules for buildings. European Committee for Standardization, Brussels, 2005.
[26] EN 1998-2. Eurocode 8: Design of structures for earthquake resistance, Part 2: Bridges. European Committee for Standardization, Brussels, 2005.
[27] EN 15129. Anti-seismic devices. European Committee for Standardization, Brussels, 2009.
[28] EN 1337-3. Structural bearings – Part 3: Elastomeric bearings. Brussels: European Committee for Standardization, Brussels, 2005.
[29] ASCE/SEI 41-13. Seismic Rehabilitation of Existing Buildings, American Society of Civil Engineers (ASCE), Reston, Virginia, 2014.
[30] Manos GC, Mitoulis SA, Sextos A. A knowledge-based software for the preliminary design of seismically isolated bridges. Bulletin of Earthquake Engineering 2012; 10 (3): 1029–1047.
[31] Mata P, Boroschek R, Barbat AH, Oller S. High damping rubber model for energy dissipating devices. Journal of Earthquake Engineering 2007; 11 (2): 231-256.
[32] Ahmadi HR, Fuller KNG, Muhr AH. Predicting Response of Non-Linear High Damping Rubber Isolating Systems. In Eleventh World Conference on Earthquake Engineering, Elsevier Science Ltd, 1996.
[33] Razzaq MK, Bhuiyan AR, Okui Y, Mitamura H, Imai T. Effect of rubber bearings modeling on seismic response of base isolated highway bridge. In 7th CUEE and 5th ICEE Joint Conference (Vol. 7), 2010.
[34] Jara JM, Raya G, Olmos BA, Martinez G. Applicability of equivalent linearization methods to irregular isolated bridges. Engineering Structures 2017; 141: 495–511.
[35] Olmos B, Roesset J. Inertial interaction effects on deck isolated bridges. Bulletin of Earthquake Engineering 2012; 10 (3): 1009-1028.
[36] Ucak A, Tsopelas P. Effect of soil-structure interaction on seismic isolated bridges. Journal of Structural Engineering 2008; 134 (7): 1154-1164.
[37] Dezi F, Carbonari S, Tombari A, Leoni G. Soil-structure interaction in the seismic response of an isolated three span motorway overcrossing founded on piles. Soil Dynamics and Earthquake Engineering 2012, 41, 151-163.
[38] EN 1991-2. Eurocode 1: Actions on structures - Part 2: Traffic loads on bridges. European Committee for Standardization, Brussels, 2003.
[39] McKenna F, Fenves GL, Scott MH. OpenSees: open system for earthquake engineering simulation. Pacific Earthquake Engineering Center, University of California, Berkeley, 2006.
[40] Kappos AJ, Saiidi MS, Aydinoglu MN, Isakovic T. Seismic design and assessment of bridges, inelastic methods of analysis and case studies. In: Geotechnical, geological and earthquake engineering, Springer, 2012.
[41] Makris N, Badoni D, Delis E, Gazetas G. Prediction of observed bridge response with soil–pile-structure interaction. Journal of Structural Engineering 1994; 120(10): 2992–3011.
[42] Dezi F, Carbonari S, Leoni G. A model for the 3D kinematic interaction analysis of pile groups in layered soils. Earthquake Engineering & Structural Dynamics 2009; 38(11): 1281-1305.

[43] Carbonari S, Morici M, Dezi F, Gara F, Leoni G. Soil-structure interaction effects in single bridge piers founded on inclined pile groups. Soil Dynamics and Earthquake Engineering 2017; 92, 52-67.
[44] Dezi F, Carbonari S, Leoni G. Lumped parameter model for the time-domain soil-structure interaction analysis of structures on pile foundations, Proceedings of ANIDIS, 15° Convegno Nazionale - L'ingegneria sismica in Italia, Padova, 2013.
[45] Koh CG, Kelly JM. Effects of axial load on elastomeric isolation bearings. EERC/UBC 86/12, Earthquake Engineering Research Center, University of California, Berkeley, 1987.
[46] Warn GP, Whittaker AS, Constantinou MC. Vertical stiffness of elastomeric and lead-rubber seismic isolation bearings. Journal of Structural Engineering 2007; 133(9): 1227-1236.
[47] Kelly JM. Earthquake-resistant design with rubber. Springer, London, 1997.
[48] Kelly JM, Konstantinidis D. Mechanics of Rubber Bearings for Seismic and Vibration Isolation. John Wiley & Sons, Ltd, 2011.
[49] Tubaldi E, Dall'Asta A. A design method for seismically isolated bridges with abutment restraint. Engineering Structures 2011; 33 (3): 786–795.
[50] Cardone D. Displacement limits and performance displacement profiles in support of direct displacement ‐ based seismic assessment of bridges, Earthquake Engineering & Structural Dynamics 2014; 43(8), 1239-1263.
[51] Iervolino I, Galasso C, Cosenza E. REXEL: computer aided record selection for code-based seismic structural analysis. Bulletin of Earthquake Engineering 2010; 8(2): 339-362.